IEEE Access
Multidisciplinary | Rapid Review | Open Access Journal

IEEE VEHICULAR TECHNOLOGY SOCIETY SECTION

Received 9 January 2024, accepted 29 January 2024, date of publication 1 February 2024, date of current version 8 February 2024.

Digital Object Identifier 10.1109/ACCESS.2024.3361399

RESEARCH ARTICLE

Traffic Improvement in Manhattan Road Networks With the Use of Parallel Hybrid Biobjective Genetic Algorithm

ANDRANIK S. AKOPOV[1,2,3], (Member, IEEE), AND LEVON A. BEKLARYAN[1,2]
[1]Russian Academy of Sciences, Central Economics and Mathematics Institute, 117418 Moscow, Russia
[2]Moscow Institute of Physics and Technology, 141701 Moscow, Russian
[3]MIREA—Russian Technological University, 119454 Moscow, Russian

Corresponding author: Andranik S. Akopov (andranik.s.akopov@ieee.org)

This work was supported by the Russian Scientific Foundation (RSF) under Project 23-11-00080.

ABSTRACT There are many reasons for traffic congestions such as the ''stop-and-go wave effect'', periodic increase in intensity of vehicle and pedestrian traffic (''rush hours''), frequent maneuvering, uncontrolled pedestrians' movement on road crossings and other factors. This paper considers the problem of biobjective optimization and rebalancing of vehicles' and pedestrians' flows with the use of Manhattan road networks (MRNs) with smart traffic lights (STLs) as the case study of intelligent transportation system (ITS). For this purpose, we have studied the possibilities of applying STLs to control of traffic in large-scale road networks providing a speed harmonization and traffic prioritization between vehicles and pedestrians. The considered multiagent system (MAS) includes agent vehicles, agent pedestrians and agent lights that interact with each other according with given rules (e.g., V2V, V2P, V2I). Such STLs use information on the traffic structure and its density to switch signals at each moment in time. In the non-stationary mode with a periodic traffic intensity to provide the analysis of traffic flows done by STLs it has been suggested to use the fuzzy clustering algorithm aggregated with the density-based spatial clustering algorithm (FCA-DBSCAN). At the uniform motion fixed durations of phases set up for STLs that computed individually with use of the suggested parallel hybrid genetic algorithm (BORCGA-BOPSO). The proposed algorithm combine the use of the Biobjective Real-Coded Genetic Algorithm (BORCGA) for an evolutionary search based on heuristic operators and the Biobjective Particle Swarm Optimization Algorithm (BOPSO) based on simple way to search for optimal solutions. The approach allows to improve significantly the time-efficiency of seeking optimal individualised STLs' characteristics while keeping up their quality. Moreover, the ITS based on STLs with parameters optimized with the BORCGA-BOPSO provides significant traffic improvement (i.e., a maximization of the vehicle and pedestrian outflows) in MRNs in contrast to the case of uncontrolled pedestrian crossings and using usual (i.e., non-smart) traffic lights.

INDEX TERMS Agent-based modeling, fuzzy clustering, genetic algorithms, intelligent transportation systems, large-scale road networks, Manhattan road networks, multiagent systems, multiobjective optimization, smart traffic lights, traffic improvement.

I. INTRODUCTION

Over the past two decades, several simulation-based approaches have been developed to design Intelligent Transportation Systems (ITS) (e.g., [1], [2], [3], [4], [5], [6]). Among them, using Smart Traffic Lights (STLs) providing an adaptive control of vehicles' and pedestrians' flows should be highlighted. This is one of main approaches to speed harmonization and reducing traffic jams. There is a line of research devoted to developing such STLs with the use of

The associate editor coordinating the review of this manuscript and approving it for publication was Jie Gao.

artificial intelligence techniques such as an adaptive control, neural networks and heuristic algorithms to improve road safety, reduce traffic congestions, give priority to pedestrians or cyclists during interactions between them on the crosswalk, and harmonize traffic flows (e.g., [7], [8], [9], [10], [11], [12]). At the same time, the most important problem of reducing traffic congestions using STLs should be highlighted (e.g., [13], [14], [15], [16], [17], [18]). In particular, in [15] is described the mechanism of formation and propagation of stop-and-go waves in congested freeway traffic. Using traffic lights in a connected road network can have both a positive (e.g., [17], [18]) and a negative impact on traffic due to the ''stop-and-go wave effect'' emerging before STLs [15]. The negative effect increases if STLs are too closely located near each other. At the same time, the rare use of STLs on crosswalks or too short signal cycles lengths of STLs can increase the number of collisions between pedestrians and road vehicles causing traffic conjunctions and accidents. Thus, an optimization of STLs' allocation and improving their characteristics in street road networks is an actual problem. Although, such an optimization for some local crossroads and crosswalks can be completed using known simulation-based techniques, the traffic improvement problem for the large-scale ITS such as MRNs is a relevant high-computational complexity challenge hitherto [19], [20], [21].

This study considers the possibilities of traffic improvement in MRNs with the use of the simulation-based optimization techniques such as the proposed parallel hybrid real-coded genetic algorithm (BORCGA-BOPSO). Such an approach aims to solve the biobjective optimization problem of a multiagent transportation system within of which particular trade-offs can be picked up along the Pareto frontier to maximize both a pedestrian traffic flow and a road traffic flow. It is shown how the best allocation of STLs with improved characteristics (e.g., optimized signals' cycles lengths) in the large-scale Manhattan road network can be provided with the use of the BORCGA-BOPSO. The individual decision-making systems of STLs use information on the traffic structure and its density with the use of the fuzzy clustering algorithm aggregated with the density-based spatial clustering algorithm (FCA-DBSCAN) to switch signals at each moment in time. At the same time, the base values of signals' cycles lengths including full shutdown states are computed with the BORCGA-BOPSO. Thus, the proposed approach is based on the microscopic agent-based models, spatial clustering methods and simulation-based optimization to study the traffic improvement in large-scale transportation systems such as Manhattan Road Networks (MRNs).

II. TRANSPORTATION MODEL

The proposed transportation model considers the behavior of vehicles in MRNs with multiple crosswalks which are controlled and uncontrolled depending on states of traffic lights. Unlike the previous models intended to improve maneuverability (e.g., [5], [6]), the suggested model focuses on seeking for conditions to provide the balance of the interests between drivers and pedestrians and maximizing appropriate traffic flows.

A. MODEL CONCEPT

The proposed model is based on the concept and methods of the phenomenological approach suggested in works [22], [23], [24]. The main feature of the phenomenological approach is modeling human behavior under the influence of social forces, for example, a pedestrians' desire to keep a comfortable distance between each other when moving, their readiness to reduce the distance in the high-density crowd up to the given limit, humans' intention to avoid mutual collisions and areas with a large number of any obstacles (e.g., other pedestrians and vehicles). Such principles can be also taken to modeling drivers' behavior with consideration of the pedestrian priority in crosswalks and the need to avoid contacts. Also, it is necessary to consider traffic rules (e.g., the requirement of braking when a pedestrian appears, movement controlled by traffic lights, etc.) and traffic psychology. For instance, when drivers are braking before a traffic light they gradually increase the distance between each other causing the ''stop-and-go wave effect''. If the distance is reduced below the threshold level in high-density traffic, a panic occurs with efforts of impatient drivers to extend their personal spaces, i.e., the ''turbulence effect'' is appeared [6]. As a result, impatient driving habits lead to wide-moving jam flow in the high density [25]. The spatial variability of vehicle densities under the influence of traffic lights and pedestrian dynamics can be modeled with the use of different techniques.

The first group of methods is based on macroscopic traffic simulations (e.g., [25], [26], [27], [28], [29], [30], [31]). Macroscopic models consider road movement as aggregated traffic flows. Macroscopic models allow simulating large road networks, but they have no ability to capture individual behavior of road users and their influence on the system. In particular, there is suggested well-known ''two-fluid model of town traffic'' in the fundamental work [25]. This model is based on ideas formulated in a kinetic theory of multilane traffic. Within the approach two fluids are taken to consist of moving cars and cars stopped as a result of traffic conditions. It is assumed that the average speed of moving vehicles is proportional to the proportion of moving vehicles increased to a degree that reflects the ''quality'' of traffic. The important advantage of such an approach is the use of the first-order ordinary differential equations set can describe the behavior of a whole transportation system without the need to detail it. Further, in [31] a new macroscopic model was proposed to characterize the physiological and psychological response of drivers to changes in the traffic flow. However, the results obtained with macroscopic simulations are too rough and they do not have spatial referencing (i.e., precise locations of the ITS agents). The second group of methods is based on mesoscopic traffic simulations (e.g., [32], [33], [34], [35],

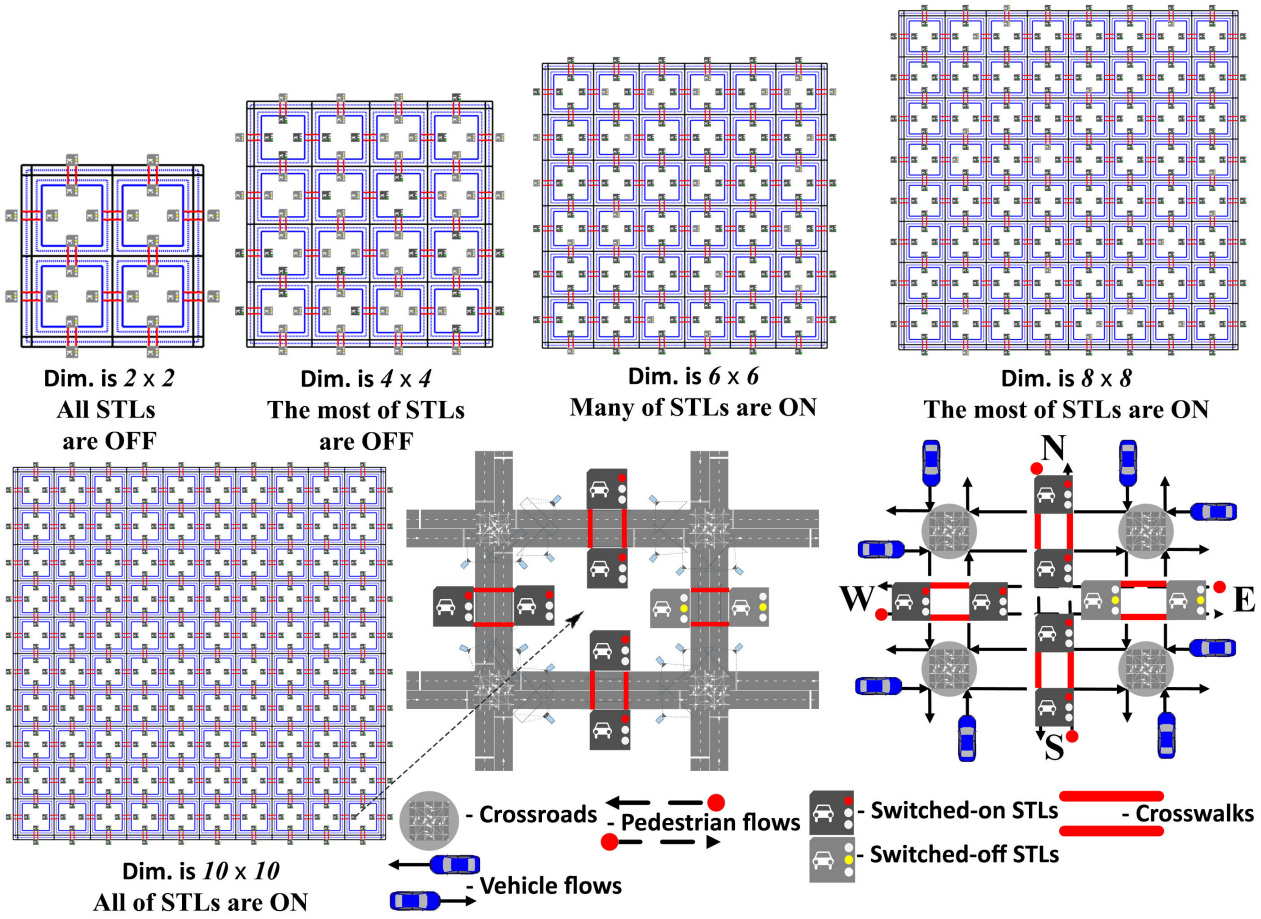

FIGURE 1. Illustration of the ITS based on Manhattan road networks with different characteristics.

[36]) Mesoscopic models are not able to describe the interaction between vehicles and their behaviors at a high level of detail. Mainly, mesoscopic traffic models aim to fill the gap between microscopic and macroscopic models. For instance, in [35] is presented the mesoscopic model developed with the agent-based approach.The model is macroscopic at the traffic flows' level and microscopic at the individual trips' level enabling some features presented in microscopic models while inheriting the computational efficiency of macroscopic models. Nevertheless, there is no ability to build the ITS with detailed road networks and different infrastructure objects layouts (e.g., STLs).

In contrast with the first and the second groups of methods, the microscopic traffic models (e.g., [37], [38], [39]) allow simulate various scenarios of interactions between road users (e.g., V2V, V2P, V2I), reproduce important phenomena, such as the ''stop-and-go wave effect'', the ''turbulence effect'', accidents, etc. to study traffic congestions, and consider the influence of STLs' adaptive signal control, etc. The use of Graphic Processing Units (GPUs) and frameworks intended for large-scale agent-based models such as FLAME GPU allows us to significantly increase the computational efficiency of microscopic traffic models (e.g., [6], [21], [36]). In this study, we consider the original microscopic traffic model with the use of MRNs with different numbers of nodes, each of which includes four nearest intersections and pedestrian crossings. The model considers heterogenous agents (i.e., vehicles and pedestrians) and crosswalks, some of which are controlled by STLs. Such a system is illustrated in Fig. 1.

As shown in Fig. 1, the studied ITS is based on MRNs with different characteristics, for instance, when the small-scale (dim. is 2×2), the medium-scale (e.g., dim. is 6×6) or the large-scale (dim. is 10×10) dimensionality is used. Also, the different number of STLs with various signals' cycles lengths can be switched-on in various areas of the MRN that affects on traffic flows. Finally, different types of traffic intensity for arriving pedestrian and vehicle flows can be considered, for instance, spatially uniform arriving flows (i.e., in the time-independent traffic intensity) and periodic flows (i.e., in the time-dependent traffic intensity). The proposed simulation model of the movement of vehicles and pedestrians in interaction with STLs, as seen in previous models (e.g., [5], [6]) is based on a system of finite-difference equations with a variable structure. Unlike the models proposed in [5] and [6], here we studied the ITS with significantly more complex configurations, in particular, that provide the adaptive control of STLs within MRNs to maximize both pedestrian and vehicle traffic flows (Fig. 1). Also, the model considers the

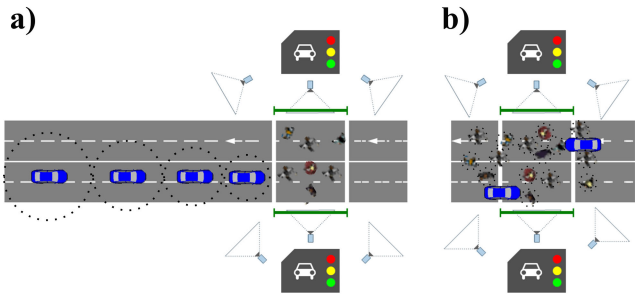

FIGURE 2. Illustration of the "stop-and-go wave effect" (a) and incomplete compliance with traffic rules (b).

behavior of drivers interacting with pedestrian flows, causing a gradual increase in the distance to the vehicle in front, which results in a wave effect of speed reduction (the "stop-and-go wave effect").

As follows from Fig. 1, in the considered ITS, two-lane traffic of vehicles is provided in all four directions, i.e., a bottom-up (the *"S-N"* direction), a top-down (the *"N-S"* direction), a left-to-right (the *"W-E"* direction), and a right-to-left (the *"E-W"* direction). At the same time, it is possible for vehicles to maneuver (rebuild) within the road (i.e., without entering the oncoming lane), in particular, when overtaking, and also in order to prevent collisions with pedestrians. With an increase in the density of the road flow relative to some agents (vehicle or pedestrian), the radius of his personal space gradually decreases up to a certain threshold level (different for pedestrians and vehicles), after overcoming which, the radius increases sharply, due to the panic that occurs in the driver and the desire to the expansion of personal space in order to avoid an emergency. The result is the "turbulence effect" (strong compression waves), which usually leads to accidents and subsequent traffic congestion. Thus, when the ensemble is moving by pedestrians and vehicles, the distance between the nearest agents must be at least the sum of the radiuses' lengths of their personal spaces. When expanding the area of the personal space of one of the agents, other agents must take this circumstance into account when maneuvering. A similar approach, based on a controlled change in the radius of the agent's personal space, is also used in the model to simulate the "stop-and-go wave effect". In particular, the value of the radius of each agent vehicle following the vehicle making a forced stop (e.g., due to a traffic light prohibiting signal) gradually increases (Fig. 2a).

On the part of pedestrians and vehicles' drivers, there is an incomplete compliance with traffic rules (e.g., [40]), which can be expressed, in particular, in the willingness to cross the road, including beyond the boundaries of the pedestrian crossing, and especially in the presence of pedestrian congestions and other obstacles on a pedestrian crossing, ready to go around a pedestrian instead of stopping, etc. (Fig. 2b).

B. MODEL DESCRIPTION

Within the phenomenological approach previously proposed in [24], human behavior (e.g., pedestrians, drivers, etc.) is modeled when taking into account their psychology and the influence of the crowd (for pedestrians) or traffic jams (for drivers). Agents of both types react to changes in the density of the surrounding space, tend not to violate the personal space of other agents, try to bypass obstacles, etc. At the same time, the spatial dynamics of pedestrians and vehicles can be described by a system of finite-difference equations with the variable structure that considers possible interactions between different agents and transportation infrastructure (e.g., agent pedestrians, agent vehicles, smart traffic lights, etc.). Below, a brief abstract description of the developed model is presented. The notations introduced are presented in Appendix A.

The traffic capacity of the studied ITS should be estimated with different ways for pedestrian and vehicle traffic flows due to a significant difference in the motion speed of the agents belonging to appropriate types.

The traffic capacity of pedestrian flows can be estimated as the total number of the MRN's nodes passed by all i^{ths} agent pedestrians, $(i \in I)$bymoment $|T|$:

$$P = \sum_{t_k=1}^{|T|} \sum_{i=1}^{|I|} a_i(t_k) \tag{1}$$

where

$$a_i(t_k) = \begin{cases} \left\lfloor \dfrac{x_i(t_{k-1}) - \underline{x}}{\hat{l}} + 0.5 \right\rfloor, & \text{if } s_i(t_{k-1}) = 1, \\ \left\lfloor \dfrac{\bar{x} - x_i(t_{k-1})}{\hat{l}} + 0.5 \right\rfloor, & \text{if } s_i(t_{k-1}) = 2, \\ \left\lfloor \dfrac{y_i(t_{k-1}) - \underline{y}}{\hat{l}} + 0.5 \right\rfloor, & \text{if } s_i(t_{k-1}) = 3, \\ \left\lfloor \dfrac{\bar{y} - y_i(t_{k-1})}{\hat{l}} + 0.5 \right\rfloor, & \text{if } s_i(t_{k-1}) = 4. \end{cases} \tag{2}$$

In (2), the component of 0.5 is necessary for rounding up to the next natural number, which determines the node number of the MRN.

The traffic capacity of vehicle flows can be estimated as the total number of $\tilde{i}^{ths}$ agent vehicles, $(\tilde{i} \in \tilde{I})$ that left the traffic area of the MRN by the time $|T|$:

$$V = \sum_{t_k=1}^{|T|} \sum_{\tilde{i}=1}^{|\tilde{I}|} \tilde{a}_{\tilde{i}}(t_k), \tag{3}$$

where

$$\tilde{a}_{\tilde{i}}(t_k) = \begin{cases} 1, & \text{if I is true,} \\ 0, & \text{if II is true,} \end{cases}$$

where

I. $(\tilde{x}_{\tilde{i}}(t_k) > \bar{x}$ *and* $\tilde{s}_{\tilde{i}}(t_{k-1}) = 1)$ *or* $(\tilde{x}_{\tilde{i}}(t_k) < \underline{x}$ *and* $\tilde{s}_{\tilde{i}}(t_{k-1}) = 2)$, *which means the agent vehicle ran off the MRN boundaries moving along the horizontal lanes (**"W-E"**, **"E-W"**),*

II. $(\tilde{y}_{\tilde{i}}(t_k) > \bar{y}$ *and* $\tilde{s}_{\tilde{i}}(t_{k-1}) = 3)$ *or* $(\tilde{y}_{\tilde{i}}(t_k) < \underline{y}$ *and* $\tilde{s}_{\tilde{i}}(t_{k-1}) = 4)$, *which means the agent vehicle ran off the MRN boundaries moving along the vertical lanes (**"S-N", "N-S"**).*

The spatial dynamics of the j^{th} *agent,* $(j \in I \bigcup \tilde{I})$ *for the ITS based on the MRN can be given using the following system of finite-difference equations with the variable structure at moment* t_k, $(t_k \in T)$:

$$x_j(t_k) = \begin{cases} x_j(t_{k-1}), & \text{: if III is true,} \\ x_j(t_{k-1}) + \lambda\delta_j(t_{k-1})g_j, & \text{: if IV is true,} \\ x_j(t_{k-1}) + \lambda\delta_j(t_{k-1})g_j & \\ \times \cos\left(\pm\beta_{j\xi}(t_{k-1})\right) & \\ +\delta_j(t_{k-1})\frac{\kappa}{d_j(t_{k-1})} & \\ \times \cos\gamma_{j\xi}(t_{k-1}), & \text{: if V is true,} \end{cases} \tag{4}$$

$$y_j(t_k) = \begin{cases} y_j(t_{k-1}), & \text{: if VI is true,} \\ y_j(t_{k-1}) + \lambda\delta_j(t_{k-1})g_j, & \text{: if VII is true,} \\ y_j(t_{k-1}) + \lambda\delta_j(t_{k-1})g_j & \\ \times \sin\left(\pm\beta_{j\xi}(t_{k-1})\right) & \\ +\delta_j(t_{k-1})\frac{\kappa}{d_j(t_{k-1})} & \\ \times \sin\gamma_{j\xi}(t_{k-1}), & \text{: if VIII is true,} \end{cases} \tag{5}$$

where

III. $s_j(t_{k-1}) \in \{3,\ 4\}$ *or* $(s_j(t_{k-1}) \in \{1,\ 2\}$ *and* $\mu_j(t_k) = 0)$, *which means the agent is moving in a vertical direction ("S-N" or "N-S") or the agent is in the zone of action of a traffic light prohibiting signal when moving in a horizontal direction of the MRN;*

IV. $s_j(t_{k-1}) \in \{1,\ 2\}$ *and* $\tilde{d}_{j\xi}(t_{k-1}) > \hat{r}_j(t_k) + \hat{r}_\xi(t_k)$ *and* $\mu_j(t_k) = 1$, *which means the agent is moving in a horizontal direction ("W-E" or "E-W") and there is not any obstacle on its path as another agent (a vehicle or pedestrian) and the traffic is allowed for the agent in motion on regulated sections of the MRN;*

V. $s_j(t_{k-1}) \in \{1,\ 2\}$ *and* $\tilde{d}_{j\xi}(t_{k-1}) \le \hat{r}_j(t_k) + \hat{r}_\xi(t_k)$ *and* $\mu_j(t_k) = 1$, *which means the agent is moving in a horizontal direction ("W-E" or "E-W") and there is an obstacle on its path as another agent (a vehicle or pedestrian) and the traffic is allowed for the agent in motion on regulated sections of the MRN*;

VI. $s_j(t_{k-1}) \in \{1,\ 2\}$ *or* $(s_j(t_{k-1}) \in \{3,\ 4\}$ *and* $\mu_j(t_k) = 0)$, *which means the agent is moving in a horizontal direction ("W-E" or "E-W") or the agent is located in the zone of action of a traffic light prohibiting signal when moving vertically*;

VII. $s_j(t_{k-1}) \in \{3,\ 4\}$ *and* $\tilde{d}_{j\xi}(t_{k-1}) > \hat{r}_j(t_k) + \hat{r}_\xi(t_k)$ *and* $\mu_j(t_k) = 1$, *which means the agent is moving in a vertical direction ("S-N" or "N-S") and there is not any obstacle on its path as another agent (a vehicle or pedestrian) and the traffic is allowed for the agent in motion on regulated sections of the road network;*

VIII. $s_j(t_{k-1}) \in \{1,\ 2\}$ *and* $\tilde{d}_{j\xi}(t_{k-1}) \le \hat{r}_j(t_k) + \hat{r}_\xi(t_k)$ *and* $\mu_j(t_k) = 1$, *which means the agent is moving in a vertical direction ("W-E" or "E-W") and there is an obstacle on its path as another agent (a vehicle or pedestrian) and the traffic is allowed for the agent in motion on regulated sections of the road network.*

Unlike pedestrians, agent vehicles can maneuver, in particular, change lanes, avoid traffic jams, etc. In this case, system (4)-(5) can be easily modified to consider the specific behavior of vehicles at the microscopic level by including additional equations of motion, conditions and restrictions.

Thus, the main problem of optimal control of the studied ITS can be formulated as follows.

Problem A. *The need to maximize the pedestrian and vehicle traffic flows in the Manhattan road network by the sets of control parameters:* $\{\tau_{1l}(t_k), \tau_{2l}(t_k), \tau_{3l}(t_k),\ \psi_l(t_k)\}_{k=1}^{|T|}$ *and* $\{c_l,\ \varphi_l,\ \eta_l\}$:

$$\begin{cases} \max\limits_{\{\tau_{1l}(t_k),\tau_{2l}(t_k),\tau_{3l}(t_k),\ \psi_l(t_k)\}_{k=1}^{|T|},\ \{|C_l|,\ \varphi_l,\ \eta_l\}} P \\ \max\limits_{\{\tau_{1l}(t_k),\tau_{2l}(t_k),\tau_{3l}(t_k),\ \psi_l(t_k)\}_{k=1}^{|T|},\ \{|C_l|,\ \varphi_l,\ \eta_l\}} V \end{cases} \tag{6}$$

s.t.:

$$\underline{\tau}_1 \le \tau_{1l}(t_k) \le \bar{\tau}_1,\ \underline{\tau}_2 \le \tau_{2l}(t_k) \le \bar{\tau}_2,$$
$$\underline{\tau}_3 \le \tau_{3l}(t_k) \le \bar{\tau}_3,\ \psi_l(t_k) \in \{0,\ 1\},$$
$$\underline{c} \le |C_l| \le \bar{c},\ \underline{\varphi} \le \varphi_l \le \bar{\varphi},\ \underline{\eta} \le \eta_l \le \bar{\eta},$$
$$l \in L,\ t_k \in T.$$

Here, $\{\underline{\tau}_1, \underline{\tau}_2, \underline{\tau}_3\}$, $\{\bar{\tau}_1, \bar{\tau}_2, \bar{\tau}_3\}$ are values of lower and upper limits of STLs' signal cycles lengths, $\{\underline{c},\ \underline{\varphi},\ \underline{\eta}\}$, $\{\bar{c},\ \bar{\varphi},\ \bar{\eta}\}$ are values of lower and upper limits of main parameters of the adaptive algorithm that is used to switch STLs' signals.

Problem A can be classified to the large-scale biobjective optimization problems, where values of objective functions are computed as a result of simulation modeling (i.e., the "simulation-based optimization"). Therefore, for solving such a complex problem, it is proposed that we use the developed hybrid genetic algorithm BORCGA-BOPSO in combination with the FCA-DBSCAN clustering algorithm. BORCGA-BOPSO is used to compute the base values of the control parameters $\{\tau_{1l}(t_1), \tau_{2l}(t_1), \tau_{3l}(t_1),\ \psi_l(t_1)\}$ for each l^{th} STL, $(l \in L)$ at the initial moment t_1, $(t_1 \in T)$. FCA-DBSCAN is used to correct STLs' signal cycles lengths, force switching STLs if necessary, and get the improved values of control parameters $\{\tau_{1l}(t_k), \tau_{2l}(t_k), \tau_{3l}(t_k),\ \psi_l(t_k)\}_{k=1}^{|T|}$ for each l^{th} STL, $(l \in L)$ at moment t_k, $(t_k \in T)$.

At the same time, there is the possibility to pick up alternatives along the approximated Pareto frontiers to provide the better prioritization of pedestrian and vehicle traffic flows.

C. CONTROL OF SMART TRAFFIC LIGHTS

In previous work [41] an approach to adaptive control of traffic signals on crosswalks has been proposed with the use of one segment of the "Manhattan Lattice" as the case study. To control of STLs within MRNs a novel adaptive algorithm FCA-DBSCAN is developed and represented here. The algorithm is based on fuzzy clustering techniques (FCA),

firstly proposed in [42], and the density-based spatial clustering algorithm (DBSCAN) [43]. DBSCAN is used to provide non-random initialization of the membership matrix in FCA considering the features of agents' spatial location, in particular, marking as outliers agent vehicles that lie alone in low-density regions.

After executing the DBSCAN, the membership matrix (M'_0) became as follows:

$$M'_0 = \begin{pmatrix} m'_{11} & \dots & m'_{1N} \\ \vdots & \ddots & \vdots \\ m'_{c1} & \dots & m'_{cN} \end{pmatrix}, \tag{7}$$

where $m_{c_l\tilde{i}} \in \{0,\ 1\}$, $\tilde{i} \in \tilde{I}, l \in L$ and each column of the matrix has precisely one elements having value equal to 1). To obtain the initial membership matrix needed for fuzzy clustering, the following conversion is used:

$$m_{c_l\tilde{i}} = \frac{m'_{c_l\tilde{i}} + \lambda_{c_l\tilde{i}}}{\sum_{c_l=1}^{|C_l|} m'_{c\tilde{i}} + \lambda_{c_l\tilde{i}}}, \lambda_{c\tilde{i}} = \frac{\frac{A+1}{\theta_{c_l\tilde{i}}} - 1\frac{\theta_{c\tilde{l}}}{\theta_{c_l\tilde{i}}}}{A+\frac{\theta_{c_l\tilde{i}}}{\pi}}{1+\frac{1}{A}}. \tag{8}$$

Here,

- $C_l = \{c_{l1},\ c_{l2},\ \dots,\ c_{|C_l|}\}$, $l \in L$ is the set of indices of clusters related to the l^{th} STL, where $|C_l|$ is the total number of the STL's clusters;
- $\theta_{\tilde{i}}$, $\tilde{i} \in \tilde{I}$ is the angle between the radius vector of the $\tilde{i}^{th}$ agent vehicle and the radius vector of the cluster center that it belonged to as a result of the execution of *DBSCAN;*
- $\theta_{c_l\tilde{i}}$, $c_l \in C_l,\ \tilde{i} \in \tilde{I},\ c_l \neq \tilde{i}, l \in L$ is the angle between the radius vector of the $\tilde{i}^{th}$ agent vehicle and the radius vector of the c_l^{th} cluster center;
- $A \in (0,\ 1]$ is the compensation coefficient.

With the use of DBSCAN each agent vehicle contributes to the traffic density as a function of its closeness to the cluster center. As a result, the spatial traffic density can be considered in control of STLs. At the same time, FCA allows adjusting the clustering results considering additional traffic features, such as vehicles' velocities and their closeness to the STL (i.e., vehicles having a higher speed and located closer to the STL are to be associated to one cluster with more probability, increasing its density). When the ratio between the number of pedestrians located near to the controlled crosswalk and the number of vehicles in the cluster closest to the STL exceeds the given threshold, the STL's signal is force switched to ''red''. Thus, the proposed algorithm based on the FCA-DBSCAN technique is used to correct STLs' signal cycles lengths. It is presented in **Algorithm 1** in a compact form and illustrated in Fig. 3.

The FCA-DBSCAN technique can serve as a failsafe to prevent both the excessive pedestrian buildups and to avoid traffic congestions near the STL depending on which of road users are prevailed with taking into account the structure of traffic flows (i.e., densities, speeds, gaps between clusters, etc.). Moreover, the use of the FCA-DBSCAN has the secondary effect of modulating the cycle lengths, i.e., such STLs provide adjusting the cycle lengths which initial values can be computed with the use of the proposed parallel hybrid biobjective genetic algorithm (BORCGA-BOPSO).

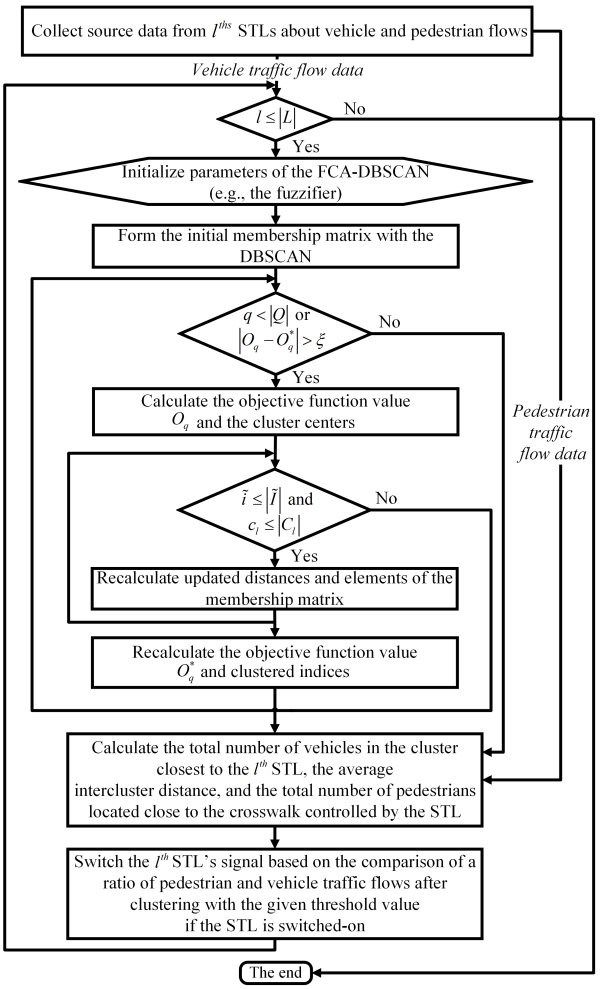

FIGURE 3. Illustration of the FCA-DBSCAN technique used to control STLs.

where,

IX. $\left(\frac{\tilde{P}_l(t_{k-1})}{\tilde{V}_l(t_{k-1})\left(\tilde{D}_l(t_{k-1})\right)^{-\upsilon}} > \varphi_l \text{ and } s_l^*(t_{k-1}) = 3\right)$ or $(t_k > t_{k-1} + \tau_{l2}(t_1) + \tau_{l3}(t_1)$ and $s_l^*(t_{k-1}) = 3)$,

X. $\left(\frac{\tilde{P}_l(t_{k-1})}{\tilde{V}_l(t_{k-1})\left(\tilde{D}_l(t_{k-1})\right)^{-\upsilon}} < \varphi_l \text{ and } s_l^*(t_{k-1}) = 1\right)$ or $(t_k > t_{k-1} + \tau_{l2}(t_1) + \tau_{l1}(t_1)$ and $s_l^*(t_{k-1}) = 1)$.

Here,

- $q \in Q$ is the index of iterations of the FCA-DBSCAN, where $Q = \{1, 2, \dots, |Q|\}$, where $|Q|$ is the total number of iterations of the FCA-DBSCAN;
- $\{O_q,\ O_q^*\}$, $q \in Q$ are values of the loss function computed at the q^{th} iteration;
- $\tilde{d}_{\tilde{i}c_l}$, $\tilde{i} \in \tilde{I}, c_l \in C_l, l \in L$ is the base-weighted Euclidian distance between the $\tilde{i}^{th}$ agent vehicle and the $c_l{}^{th}$ cluster of the l^{th} STL;

Algorithm 1 Control Algorithm for Smart Traffic Lights Based on FCA-DBSCAN

Form the initial membership matrix with DBSCAN
Initialize the FCA parameters (e.g., the fuzzifier)
for $l \leftarrow 1$ **to** $|L|$ **do**
  do
    $O_q \leftarrow$ CalculateObjectiveFunction$(\tilde{i} \in \tilde{I})$
    $C_l \leftarrow$ CalculateClusterCenters$(\tilde{i} \in \tilde{I})$
    for $\tilde{i} \leftarrow 1$ **to** $\left|\tilde{I}\right|$ **do**
      for $c_l \leftarrow 1$ **to** $|C_l|$ **do**
        $\tilde{d}_{\tilde{i}c_l} \leftarrow \sqrt{(x_{\tilde{i}} - x_{\tilde{c}_l})^2 + (y_{\tilde{i}} - y_{\tilde{c}_l})^2}$
        $\tilde{d}_{\tilde{i}c_l} \leftarrow \tilde{d}_{\tilde{i}c_l} \frac{e^{\tilde{a}\left(w_1\left|g_{\tilde{i}} - g_{c_l}\right| + w_2\left|d^*_{il} - d^*_{c_l l}\right|\right)}}{e^{\tilde{a}}}$
        $U_{\tilde{i}c_l}(q) \leftarrow \frac{1}{(\tilde{d}_{\tilde{i}c_l})^{\frac{2}{\tilde{m}-1}}}$
      end
    end
    $\hat{C}_l \leftarrow$ RecalculateClusterIndexes$(\tilde{i} \in \tilde{I})$
    $O^*_q \leftarrow$ CalculateObjectiveFunction$(\tilde{i} \in \tilde{I})$
    $q \leftarrow q + 1$
  while $q < Q$ *or* $\left|O_q - O^*_q\right| > \xi$
end

`CalculateObjectiveFunction` $\left(\tilde{i} \in \tilde{I}\right)$

$O_q \leftarrow 0$
for $\tilde{i} \leftarrow 1$ **to** $|I|$ **do**
  for $c \leftarrow 1$ **to** $|C|$ **do**
    $(\tilde{d}_{\tilde{i}c_l})^2 \leftarrow (x_{\tilde{i}} - x_{\tilde{c}_l})^2 + (y_{\tilde{i}} - y_{\tilde{c}_l})^2$
    $(\tilde{d}_{\tilde{i}c_l})^2 \leftarrow (\tilde{d}_{\tilde{i}c_l})^2 \left(\frac{e^{\tilde{a}\left(w_1\left|g_{\tilde{i}} - g_{c_l}\right| + w_2\left|d^*_{il} - d^*_{c_l l}\right|\right)}}{e^{\tilde{a}}}\right)$
    $O_q \leftarrow O_q + U^{\tilde{m}}_{\tilde{i}c_l}\left(\tilde{d}_{\tilde{i}c_l}\right)^2$
  end
end

`SwitchSmartTrafficLights`

for $l \leftarrow 1$ **to** $|L|$ **do**
  if *IX is true* **then**
    Switch the STL's signal to $s^*_l(t_{k-1}) = 1$.
  end
  if *X is true* **then**
    Switch the STL's signal to $s^*_l(t_{k-1}) = 3$.
  end
end

- $U_{\tilde{i}c_l}(q), \tilde{i} \in \tilde{I}, c_l \in C_l, q \in Q$ is the membership matrix defined for the i^{th} individual and the ${c_l}^{th}$ cluster of the l^{th} STL at the iteration q;
- $\tilde{m}$ is the fuzzifier that determines the level of cluster fuzziness ($\tilde{m} > 1$);
- $\tilde{a}$, w_1, w_2 are weights that define the significance of different characteristics of vehicle traffic (e.g., the speed, closeness to the STL, etc.) in fuzzy clustering, $w_1 + w_2 = 1, \tilde{a} \geq 1$;
- $g_{c_l}, d^*_{c_l l}$ are the motion speed of agent vehicles and their distances to the nearest STL averaged over members of the ${c_l}^{th}$ cluster, $(c_l \in C_l)$ of the l^{th} STL, $(l \in L)$;
- ξ is the accuracy of the FCA-DBSCAN (a small number);
- $\tilde{V}_l(t_{k-1})$, $\tilde{D}_l(t_{k-1})$, $l \in L$ are the total number of vehicles in the cluster closest to the l^{th} STL and the average intercluster distance (for traffic in the monitoring area of the l^{th} STL) at moment t_{k-1}, $(t_{k-1} \in T)$;
- $\tilde{P}_l(t_{k-1})$, $l \in L$ is the total number of pedestrians located close to the crosswalk controlled by the l^{th} STL at moment t_{k-1}, $(t_{k-1} \in T)$;
- υ is the coefficient of significance of the average intercluster distance in traffic flows controlled by STLs.

If the STL is switched-off, the FCA-DBSCAN technique is not used to control signals. In this case, the traffic light can be considered as a non-smart and its crosswalk is uncontrolled. Within the model, the switched-off STL is a traffic light with a flashing amber signal that allows movement for all road users.

III. PARALLEL HYBRID BIOBJECTIVE REAL-CODED GENETIC ALGORITHM

A novel parallel hybrid biobjective real-coded genetic algorithm (BORCGA-BOPSO) has been developed to provide maximization of vehicle and pedestrian traffic in MRNs. The proposed hybrid algorithm combine the use of the Biobjective Real-Coded Genetic Algorithm (BORCGA) for an evolutionary search based on heuristic operators (e.g., a crossover and mutation) and the Biobjective Particle Swarm Optimization Algorithm (BOPSO) based on simple way to search for optimal solutions. Such an approach aims to reducing the required number of recalculations of objective functions each iteration of which is computationally expensive. That is especially relevant for MRNs with multiple nodes, crosswalks and STLs where the objective functions (e.g., the traffic capacity of pedestrian and vehicle flows) are computed as results of large-scale agent-based simulation modeling.

A. RELATED WORKS

Particle Swarm Optimization (PSO) is population-based stochastic optimization algorithm suggested firstly in [44] and [45] to solve the continuous nonlinear single-objective

optimization problems. PSO can be applied to improve traffic flow. For instance, to forecast short-term traffic flows, a PSO-Bi-LSTM model based on the combination of PSO and Bidirectional-Long Short-Term Memory (Bi-LSTM) neural network is developed in [46]. At the same time, the Biobjective Particle Swarm Optimization (BOPSO) [47], Multiobjective PSO (MOPSO) [48], Multiswarm MOPSO (MS-MOPSO) [49] and their various modifications (e.g., [50], [51], [52]) have been developed. Such approaches use the concept of Pareto dominance to determine the direction of movement in decision space for particles and save previously found nondominated vectors in a global archive that is later used by other particles to guide their own search. The important advantage of PSO in comparison with genetic algorithms (GAs) is a high performance due to no need to operate with the large population of potential decisions through a selection of individuals, mutation, crossover and updating the population to provide an evolutionary search. Each particle contains a single vector of potential decisions the velocity of which should be update using inertia weighs techniques (i.e., guides) towards the best global and local solutions in the PSO. At the same time, known drawbacks of the PSO are the premature convergence, difficulties of controlling the PSO parameters and the improper velocity adjustment [53]. Therefore, designing a novel hybrid evolutionary algorithm allowing us to optimize different characteristics of large-scale ITS is needed.

Real-Coded Genetic Algorithms (RCGAs) are population-based bio-inspired evolutionary algorithms indented for solving large-scale singleobjective and multiobjective optimization problems. Unlike classic genetic algorithms suggested firstly in [54] and [55], RCGAs uses real-coded heuristic operators, such as a crossover (e.g., the simulated-binary crossover (SBX), Laplace crossover (LX), etc.) and a mutation (e.g., non-uniform mutation (NUM), power mutation (PM), etc.) to generate new potential decisions [56], [57], [58], [59], [60], [61]. The first important advantage of RCGAs is the possibility of searching in continuous decision space without necessary of using encoding and decoding operations for decision variables providing a more precision of obtained solutions (i.e., the level of accuracy after a decimal point) in less computational expenses. The second advantage is the ability to avoid a premature convergence due to a mutation operator which effectiveness depends on a number of factors (e.g., an execution probability). Finally, there is a number of genetic algorithms intended for biobjective and multiobjective optimization, e.g., the Strength Pareto evolutionary algorithm (SPEA) [62], SPEA2 [63], Non-dominated Sorting Genetic Algorithm - II (NSGA-II) [64], NSGA-III [65], [66], Multiobjective Evolutionary Algorithm Based on Decomposition (MOEA/D) [67], Parallel Real-Coded Genetic Algorithm Based on Fuzzy Clustering (FCGA) [5], etc. Such algorithms also use the concept of the Pareto dominance to build and compute the fitness-function and use it for the estimation of potential decisions. At the same time, the main difficulties with the use of RCGAs are caused by a necessary of multiple recalculations of objectives and the fitness function in generation of new potential decisions and updating the archive of nondominated solutions.

Both PCOs and RCGAs can be parallelized effectively with the use of the GPU architecture [21]. In particular, the particles' behavior in the PSO, as well as the evolutionary search with the use of selection, crossover, mutation and updating local populations of potential decisions in the RCGA can be can be implemented with the FLAME GPU framework and run at GPU cores. This also provides the possibility of the coupled use and hybridization of such algorithms. Although there are known some instances of such hybridization of particle swarm and genetic algorithms, for instance, HGAPSO [68], GA-PSO [69], HPSOGA [70], FSHPSO-E [71], such techniques are mainly intended for solving middle-scale single-objective optimization problems which not require effective parallelization and the application scalable real-coded heuristic operators. Therefore, the BORCGA-BOPSO has been developed, examined with the use of known test instances and applied to provide the traffic improvement in MRNs.

B. DESCRIPTION OF BORCGA-BOPSO

Consider the following general biobjective optimization problem:

$$\begin{aligned} &\min F(\mathbf{x}) = (f_1(\mathbf{x}), f_2(\mathbf{x}))\,, \\ &\text{s.t. } \mathbf{x} = (x_1, x_2, \ldots, x_n)' \in \Omega, \end{aligned} \tag{9}$$

where $\mathbf{x} = (x_1,\ x_2,\ \ldots,\ x_n)'$ is a decision variable vector with a dimension n, $\Omega = \prod_{j=1}^{n}[a_j,\ b_j]$ is the feasible region of the search space ($j = 1,\ 2,\ \ldots,\ n$ is the index of decision variables), $f_m(\mathbf{x})$ are the m^{th}-objective functions ($m = 1,\ 2$) which computed in the result of the agent-based simulation modelling and should be minimized with BORCGA-BOPSO.

As follows from (9), the developed algorithm is indented to solve minimization problems. At the same time, **Problem A** can be reduced to a biobjective minimization problem through replacing the objective functions with appropriate inverse values to use the BORCGA-BOPSO with the following reverse conversion when approximating the Pareto fronts.

The BORCGA-BOPSO combines two parallel evolutionary algorithms: the Biobjective Real-Coded Genetic Algorithm (BORCGA) and the Biobjective Particle Swarm Optimization (BOPSO) implemented with the GPU architecture. In the BORCGA local populations of individuals which consist of values of decision variables and appropriate solutions are used for evolutionary search. The best individuals are selected from each local population at the individual level of evolutionary processes. At the same time, the fitness function is used for assessing individuals' adaptations. The value of the fitness function defines the contribution of appropriate individual to the quality of the Pareto front showing the level

of its approximation accuracy improved. Since such estimation is computationally complex, in particular, it is necessary to compute the sum of Pareto strengths of all individuals that dominates the assessed individual (e.g., when using the SPEA strategy search) and compute the logarithmic hypervolume (LHV) [72], the BORCGA should be execute relatively rare mainly to improve basic nondominated solutions delivered by the BOPSO. Unlike the BORCGA, the population of particles with simple updating rules are used to determine the best potential decisions with the use of the concept of the Pareto dominance. In the BOPSO there is provided moving such particles around in the decision space based on an iteratively improving particle's positions through updating their directions and velocities. With the use of GPUs provides the parallelization of evolutionary search process both in the BORCGA and the BOPSO.

The important characteristic of the BORCGA is the fitness function, which is computed for each i_k^{th} individual ($i_k \in I_k$) of each k^{th}evolutionary process ($k \in K$) at iteration g_r, ($g_r \in G,\ r = 1,\ 2,\ \ldots\ |R|$):

$$\tilde{f}_{i_k}\left((\mathbf{x}_{i_k}(g_r)\right) = \frac{\tilde{h}_{i_k}\left((\mathbf{x}_{i_k}(g_r)\right)}{1+\tilde{w}_{i_k}\left((\mathbf{x}_{i_k}(g_r)\right)+\frac{1}{2+d_{i_k}\left((\mathbf{x}_{i_k}(g_r)\right)}}, \quad (10)$$

where

- $G = \{1,\ 2,\ \ldots,\ |G|\}$ is the set of indices of iterations of the BORCGA-BOPSO, $|G|$ is the total number of iterations;
- $K = \{1,\ 2,\ \ldots,\ |K|\}$ is the set of indices of parallel processes of evolutionary search of the BORCGA-BOPSO (i.e., complex computational procedures in the BORCGA or simple particles in the BOPSO), $|K|$ is the total number of parallel processes of evolutionary search;
- $I_k = \{1,\ 2,\ \ldots,\ |I_k|\}$, $k \in K$ is the set of indices of individuals of the k^{th} evolutionary processes of the BORCGA, $|I_k|$ is the total number of individuals;
- d_{i_k}, $i_k \in I_k$, $k \in K$ is the Euclidian distance (ED) from the i_k^{th}-individual to the nearest individual of the BORCGA;
- $\tilde{h}_{i_k}$, $i_k \in I_k$, $k \in K$is the contribution of the i_k^{th}-individual to the LHV computed based on particular solutions of the BORCGA;
- $\tilde{w}_{i_k}$, $i_k \in I_k$, $k \in K$ is the sum of Pareto strengths of all individuals that dominates the i_k^{th}-individual of the BORCGA computed at the iteration g_r, ($g_r \in G$):

$$\tilde{w}_{i_k}(g_r) = \sum_{\tilde{i}_k}^{|I_k|} \tilde{v}_{i_k\tilde{i}_k}(g_r), \quad (11)$$

where for $\tilde{i}_k$, $i_k \in I_k$, $k \in K$, $g_r \in G$ and a rule

XI. $\left(f_{\tilde{i}_k 1} \succ f_{i_k 1} \text{ and } f_{\tilde{i}_k 2} \succeq f_{i_k 2}\right)$ or $\left(f_{\tilde{i}_k 2} \succ f_{i_k 2} \text{ and } f_{\tilde{i}_k 1} \succeq f_{i_k 1}\right)$, here $\{f_{\tilde{i}_k 1},\ f_{i_k 1}\}$, $\{f_{\tilde{i}_k 2},\ f_{i_k 2}\}$ are the particular solutions of objective functions f_1 and f_2 corresponding to the i_k, ($i_k \in I_k$) and $\tilde{i}_k$, ($\tilde{i}_k \in I_k$) individuals, respectively

$$\tilde{v}_{i_k\tilde{i}_k}(g_r) = \begin{cases} 1, & \text{if XI is true} \\ 0, & \text{if XI is not true,} \end{cases} \quad (12)$$

is defined.

The values of new $j_k{}^{th}$ offspring individuals ($j_k \in I_k$) of each k^{th} evolutionary process ($k \in K$) of the BORCGA are computed with the following rules:

$$\mathbf{x}_{j_k}(g_r) = \begin{cases} MUT\left(\breve{\mathbf{x}}_{j_k}(g_{r-1})\right), & \text{if } h(0,\ 1) \le p_{mut}, \\ \breve{\mathbf{x}}_{j_k}(g_{r-1}), & \text{if } h(0,\ 1) > p_{mut}, . \end{cases} \quad (13)$$

where

$$\breve{\mathbf{x}}_{j_k}(g_{r-1}) = CROSS\left(\hat{\mathbf{x}}_{j_k}(g_{r-1})\right). \quad (14)$$

Here,

- $CROSS\left(\hat{\mathbf{x}}_{j_k}(g_{r-1})\right)$, $j_k \in I_k$, $k \in K$, $g_{r-1} \in G$ is the crossover operator (e.g., SBX, LX, etc.) executed over the decision variables $\hat{\mathbf{x}}_{j_k}(g_{r-1})$ corresponding to the best parent individuals (assessed with the use of (10)) selected from the local population of the k^{th} process at iteration g_{r-1};
- $MUT\left(\breve{\mathbf{x}}_{j_k}(g_{r-1})\right)$, $j_k \in I_k$, $k \in K$, $g_{r-1} \in G$ is the mutation operator (e.g., PM, SUM, etc.) executed over the decision variables $\breve{\mathbf{x}}_{j_k}(g_{r-1})$ with the probability of p_{mut} at iteration g_{r-1};
- $h(0,\ 1)$ is the random value uniformly distributed on the interval $[0,\ 1]$.

The following conditions should be fulfilled to update the local and global archives of nondominated solutions of the BORCGA at iteration g_r, ($g_r \in G$):

XII. $\left(f_{i_k 1} \succ f_{j_k 1}\left(\mathbf{x}_{j_k}(g_r)\right) \text{ and } f_{i_k 2} \succeq f_{j_k 2}\left(\mathbf{x}_{j_k}(g_r)\right)\right)$ or $\left(f_{i_k 2} \succ f_{j_k 2}\left(\mathbf{x}_{j_k}(g_r)\right) \text{ and } f_{i_k 1} \succeq f_{j_k 1}\left(\mathbf{x}_{j_k}(g_r)\right)\right)$ for any $\tilde{i}_k$, ($\tilde{i}_k \in I_k, k \in K, \tilde{i}_k \ne j_k$), *that means the* $\left\{f_{j_k 1}\left(\mathbf{x}_{j_k}(g_r)\right),\ f_{j_k 2}\left(\mathbf{x}_{j_k}(g_r)\right)\right\}$ *is the nondominated solution of objective functions* f_1 *and* f_2 *corresponding to the best decision* $\mathbf{x}_{j_k}(g_r)$ *obtained with the* k^{th} *evolutionary process* ($k \in K$) *of the BORCGA,*

XIII. $\left(f_{i_k 1} \succ f_{j1}\left(\tilde{\mathbf{x}}_j(g_r)\right) \text{ and } f_{i_k 2} \succeq f_{j2}\left(\tilde{\mathbf{x}}_j(g_r)\right)\right)$ or $\left(f_{i_k 2} \succ f_{j2}\left(\tilde{\mathbf{x}}_j(g_r)\right) \text{ and } f_{i_k 1} \succeq f_{j1}\left(\tilde{\mathbf{x}}_j(g_r)\right)\right)$ for any $\tilde{i}_k$, ($\tilde{i}_k \in I_k, k \in K, \tilde{i}_k \ne j$), *that means the* $\left\{f_{j1}\left(\tilde{\mathbf{x}}_j(g_r)\right),\ f_{j2}\left(\tilde{\mathbf{x}}_j(g_r)\right)\right\}$ *is the nondominated solution of objective functions* f_1 *and* f_2 *corresponding to the best decision* $\tilde{\mathbf{x}}_j(g_r)$ *obtained with all evolutionary processes of the BORCGA.*

When using the biobjective swarm algorithm (BOPSO), the velocity vector for the decision-variables is calculated, which determines the positions of the k^{ths} particles ($k \in K$) in the space of potential decisions at iteration g_r, ($g_r \in G,\ r = 1,\ 2,\ \ldots\ |R|$):

$$\mathbf{v}_k(g_r) = \theta \mathbf{v}_k(t_{r-1})$$

$$+ c_1 q(0,\ 1)(\mathbf{x}_k^*(g_{r-1}) - \mathbf{x}_k(g_{r-1})) + c_2 e(0,\ 1)\left(\tilde{\mathbf{x}}(g_{r-1}) - \mathbf{x}_k(g_{r-1})\right), \quad (15)$$

$$\mathbf{x}_k(g_r) = \begin{cases} \mathbf{x}_k(g_{r-1}) + \mathbf{v}_k(g_{r-1}), & \text{if XIV is true,} \\ \mathbf{x}_k(g_{r-1}), & \text{if XV is true,} \end{cases} \quad (16)$$

where

XIV. $\mathbf{x}_k(g_{r-1}) + \mathbf{v}_k(g_{r-1}) \in [\underline{\mathbf{x}},\ \bar{\mathbf{x}}]$,

XV. $\mathbf{x}_k(g_{r-1}) + \mathbf{v}_k(g_{r-1}) \notin [\underline{\mathbf{x}},\ \bar{\mathbf{x}}]$,

for $\mathbf{x}_k^*(g_r)$, $(k \in K,\ g_r \in G)$ the following rule:

XVI. $\left(f_{k1}\left(\mathbf{x}_k(g_{r-\xi})\right) \succ f_{k1}\left(\mathbf{x}_k^*(g_r)\right)\right.$ and $\left.f_{k2}\left(\mathbf{x}_k(g_{r-\xi})\right) \succeq f_{k2}\left(\mathbf{x}_k^*(g_r)\right)\right)$ or $\left(f_{k2}\left(\mathbf{x}_k(g_{r-\xi})\right) \succ f_{k2}\left(\mathbf{x}_k^*(g_r)\right)\right.$ and $\left.f_{k1}\left(\mathbf{x}_k(g_{r-\xi})\right) \succeq f_{k1}\left(\mathbf{x}_k^*(g_r)\right)\right)$ for any $\mathbf{x}_k(g_{r-\xi})$, $(g_{r-\xi} = 1,\ \ldots,\ g_{r-1})$ is defined, *that means the* $\left\{f_{k1}\left(\mathbf{x}_k^*(g_r)\right),\ f_{k2}\left(\mathbf{x}_k^*(g_r)\right)\right\}$ *is the nondominated solution of objective functions* f_1 *and* f_2 *corresponding to the best decision* $\mathbf{x}_k^*(g_r)$ *obtained with the* k^{th} *particle* $(k \in K)$ *of the BOPSO during the search period at iteration* g_r, $(g_r \in G)$,

and for $\tilde{\mathbf{x}}(g_r)$, $(g_r \in G)$ the following rule:

XVII. $\left(f_{k1}\left(\mathbf{x}_k(g_r)\right) \succ f_1\left(\tilde{\mathbf{x}}(g_r)\right)\right.$ and $\left.f_{k2}\left(\mathbf{x}_k(g_r)\right) \succeq f_2\left(\tilde{\mathbf{x}}(g_r)\right)\right)$ or $\left(f_{k2}\left(\mathbf{x}_k(g_r)\right) \succ f_2\left(\tilde{\mathbf{x}}(g_r)\right)\right.$ and $\left.\left(f_{k1}\left(\mathbf{x}_k(g_r)\right) \succeq f_1\left(\tilde{\mathbf{x}}(g_r)\right)\right)\right.$ for any $\mathbf{x}_k(g_r)$, $(k \in K)$ is defined, *that means the* $\left\{f_1\left(\tilde{\mathbf{x}}(g_r)\right),\ f_2\left(\tilde{\mathbf{x}}(g_r)\right)\right\}$ *is the nondominated solution of objective functions* f_1 *and* f_2 *corresponding to the best decision* $\tilde{\mathbf{x}}(g_r)$ *obtained with all particles in the current swarm of the BOPSO at iteration* g_r, $(g_r \in G)$

are fulfilled.

Here,

- $\mathbf{x}_k^*(g_{r-1})$, $\tilde{\mathbf{x}}(g_{r-1})$ are the best potential decisions chosen randomly or with guides from appropriate archives and obtained by the k^{th} particle $(j \in J)$ of the BOPSO during the search period and all particles at iteration g_r, $(g_{r-1} \in G)$;
- $q(0,\ 1)$, $e(0,\ 1)$ are random values uniformly distributed on the interval $[0,\ 1]$;
- θ, c_1, c_2 are constants of the BOPSO, the values of which, as a rule, are set in the following ranges: $\theta \in [0.4,\ 1.4]$, $c_1 \in [1.5,\ 2]$, $c_2 \in [2,\ 2.5]$.

The proposed hybrid BORCGA-BOPSO in a simplified form is given in **Algorithm 2**. All particles of the BOPSO and evolutionary processes of the BORCGA are implemented at the individual level of GPU (i.e., in parallel) and interacted with each other using a Central Processing Unit (CPU). In **Algorithm 2**, $\hat{w}$ is the frequency of alternating the use of the BORCGA and the BOPSO to search for the best potential decisions with updating archives of nondominated solutions.

Algorithm 2 Hybrid BORCGA-BOPSO

```
Initialise the global BORCGA-BOPSO parameters
  (e.g., the number of particles, processes, etc.).
Clear the local and global archives of nondominated
  solutions of BOPSO: A_k^* ← ∅ and Ã ← ∅.
Clear the local and global archives of nondominated
  solutions of BORCGA: P_k^* ← ∅ and P̃ ← ∅.
for g ← 1 to |G| do
    for k ← 1 to |K| do
        if g − ŵ ⌊g/ŵ⌋ ≠ 0 then
            Initialise the values of decision variables
              x_k using (15)–(16).
            Compute the values of objective functions
              {f_k1(x_k), f_k2(x_k)}.
            if XVI is true for x_k^* ← x_k then
                Update the local archive of
                  nondominated solutions (A_k^* ≠ ∅) of
                  BOPSO.
            end
            if XVII is true for x̃ ← x_k then
                Update the global archive of
                  nondominated solutions (Ã ≠ ∅) of
                  BOPSO.
            end
        end
        Generate offspring individuals x_{j_k}, (j_k ∈ I_k)
          using (13)–(14).
        for j_k ← 1 to |I_k| do
            Compute the value of the fitness function
              f̃_{j_k}(x_{j_k}) using (10).
            if XII is true for x_{j_k} then
                Update the local archive of
                  nondominated solutions (P_k^* ≠ ∅) of
                  BORCGA.
            end
            if XIII is true for Q_j ← x_{j_k} then
                Update the global archive of
                  nondominated solutions (P̃ ≠ ∅) of
                  BORCGA.
            end
        end
    end
    if g − ŵ ⌊g/ŵ⌋ ≠ 0 then
        Update the local and global archives of
          nondominated solutions of BORCGA with
          nondominated solutions from the local and
          global archives of BOPSO, respectively.
    end
    else
        Update the local and global archives of
          nondominated solutions of BOPSO with
          nondominated solutions from the local and
          global archives of BORCGA, respectively.
    end
end
```

C. TEST INSTANCES AND PERFORMANCE METRICS

The test instances used to examine the performance of the BORCGA-BOPSO and to estimate various performance metrics are presented in Appendix B. These test instances are characterized by different properties, including convex, nonconvex and discontinuous Pareto frontiers, and the presence of multiple decision variables ([73], [74], [75], [76], [77])).

Then the performance metrics of the BORCGA-BOPSO have been assessed in comparison with others well known parallel multiobjective optimization algorithms, also implemented using the FLAME GPU according to the most important criteria:

1) *LHV* is the logarithmic hyper volume metric, which determines the total area of the objective space covered by the approximating Pareto front. A higher value of the LHV indicates the superiority of an algorithm [72];
2) *IGD* is the inverted generational distance characterizing the distance between the Pareto front obtained using the heuristic algorithm and the reference Pareto front [78]. A lower value of the IGD indicates the superiority of an algorithm;
3) *CPF* is the Pareto front cardinality, which determines the number of different trade-offs solutions in the estimated Pareto front obtained using an evolutionary algorithm [79]. A higher value of the CFP indicates the superiority of an algorithm
4) *PT*, sec. is the processing time that spent forming the Pareto-optimal solutions [79]. It should be minimized;
5) *CPF/ PT* is the ratio of the number of obtained nondominated solutions to the process time.

At the same time, the performance of the BORCGA-BOPSO was assessed in comparison with other well-known parallel multiobjective optimization algorithms (e.g., SPEA [62], SPEA2 [63], NSGA-II [64], FCGA [5], MOPSO [47], [48], MS-MOPSO [51] also implemented using the FLAME GPU.

In Table 1, the average performance indicators of the BORCGA-BOPSO are presented in comparison with other well known multiobjective optimization evolutionary algorithms. Optimization experiments were undertaken with the use of the portative supercomputer DSWS PRO (2x Intel Xeon Silver 4114, 1x NVIDIA QUADRO RTX 6000). At the same time, there are used 100 evolutionary processes and swarm particles ($|K| = 100$) at the level of GPUs, while the total number of iterations $|T| = 100$ and $\hat{w} = 5$.

The total number of decision variables used in the test instances (Appendix B) is specified as follows:

- $n = 2$ for FT1, FT2, FT4;
- $n = 3$ for FT3,
- $n = 30$ for FT5;
- $n = 10$ for FT6.

When undertaking optimization tests any restrictions on the minimum distance between the neighboring solutions belonging to the Pareto front and the CPF were not considered.

Such important characteristics as the value ranges of the LHV and the CFP/PT that were assessed as a result the repeated multiple optimization experiments with the use of considered evolutionary algorithms and test instances are depicted in Fig. 3. When conducting experiments the same values of control parameters of parallel evolutionary algorithms were used.

As seen from Table 1 and Fig. 3 the proposed hybrid genetic algorithm BORCGA-BOPSO is comparable in terms of the processing time (PT) with the methods of fast multiobjective heuristic optimization MOPSO [47], [48], MS-MOPSO [51] and SPEA [62], and in terms of the LHV, IGD and CPF criteria with the computationally intensive algorithms NSGA-II [64] and FCGA [5].

As evident from Fig. 3, the BORCGA-BOPSO shows the improved values of the LHV and the CFP/PT for the most of test instances. Also, it is clear from Fig.3 that the BORCGA-BOPSO demonstrates the stable performance.

The sensitivity tests for the LHV and the CPF completed with the BORCGA-BOPSO is shown with Fig. 5. The tests confirm the possibility of improving values of performance metrics through both increase in the number of used core processes and sizes of their local populations. At the same time, the total number of parallel evolutionary processes and particles in swarm of the BORCGA-BOPSO is the most important.

IV. OPTIMIZATION RESULTS

A. DESIGN OF EXPERIMENTS

Further, the BORCGA-BOPSO is applied to seeking optimal solutions in the MRNs with STLs. Two scenarios of vehicle and pedestrian traffic will be studied within the optimization experiments:

- **Scenario 1:** a stationary mode when the intensity of arrival of agents into the ITS and their preferred velocities are constants;
- **Scenario 2:** a non-stationary mode with the periodic traffic intensity and variable velocity that means the intensity of arrival of agents into the ITS and their preferred speeds are time-dependent and have peaks.

The intensity of the arrival of the j^{th}-agent, $(j \in I \bigcup \tilde{I})$ into the ITS with the periodic characteristics and its velocity are computed at each moment t_k $(t_k \in T)$:

$$a_j(t_k) = \begin{cases} \tilde{a}_j(\hat{a},\ \sigma),\ \text{if } t_k \le \dfrac{1}{4}|T| \text{ or } t_k \ge \dfrac{3}{4}|T|, \\ \widehat{a}_j\ (w,\ \varsigma),\ \text{if } \dfrac{1}{4}|T| < t_k < \dfrac{3}{4}|T|, \end{cases} \tag{17}$$

$$g_j(t_k) = \begin{cases} \tilde{g}_j(\hat{g},\ \omega),\ \text{if } t_k \le \dfrac{1}{4}|T| \text{ or } t_k \ge \dfrac{3}{4}|T|, \\ \widehat{g}_j\ (h,\ \upsilon),\ \text{if } \dfrac{1}{4}|T| < t_k < \dfrac{3}{4}|T|, \end{cases} \tag{18}$$

where

- I, $\tilde{I}$ are the sets of indices of agent vesicles and agent pedestrians, respectively;
- $\tilde{a}_j(\hat{a},\ \sigma)$, $\tilde{g}_j(\hat{g},\ \omega)$ are the arrival intensities and motion speed of the j^{th} agent, $(j \in I \bigcup \tilde{I})$ setting with a normal

TABLE 1. Evaluation of performance metrics of BORCGA-BOPSO.

Performance metrics	**BORCGA-BOPSO**	Parallel biobjective evolutionary algorithm					
		SPEA	SPEA2	NSGA-II	FCGA	MOPSO	MS-MOPSO
FT1 - Binh and Korn function							
LHV	**3.845**	3.808	3.845	3.845	3.845	3.808	3.816
IGD	**0.0765**	0.0213	0.0792	0.1388	0.2841	0.0212	0.0211
CPF	**4523**	780	15060	16636	15159	848	862
PT, sec.	**78**	36	436	464	340	21	27
CPF/PT	**57.7**	21.7	34.6	35.8	44.6	39.9	32.4
FT2 - Fonseca-Fleming function							
LHV	**-0.0006**	-0.0079	-0.0003	-0.0002	-0.0002	-0.0020	-0.0020
IGD	**0.0002**	0.0004	0.0002	0.0001	0.0001	0.0009	0.0009
CPF	**1991**	84	3389	8606	8614	311	358
PT, sec.	**43**	10	90	197	272	20	23
CPF/PT	**46.0**	8.1	37.5	43.7	31.7	15.6	15.6
FT3 - Kursawe function							
LHV	**1.9075**	1.8198	1.9097	1.9092	1.9094	1.8640	1.8671
IGD	**0.0448**	0.0478	0.1549	0.0620	0.0593	0.1119	0.1111
CPF	**160**	12	256	412	399	37	44
PT, sec.	**28**	8	53	70	70	21	25
CPF/PT	**5.8**	1.4	4.9	5.9	5.7	1.8	1.8
FT4 - Poloni's two objective function							
LHV	**2.7065**	2.7055	2.7070	2.7070	2.7069	2.7059	2.7064
IGD	**0.1526**	0.2676	0.2102	0.3924	0.3194	0.1363	0.1363
CPF	**202**	77	480	486	472	107	127
PT, sec.	**28**	19	56	72	83	20	24
CPF/PT	**7.3**	4.2	8.6	6.8	5.7	5.4	5.3
FT5 - Zitzler-Deb-Thiele's function N. 3							
LHV	**0.2021**	0.2014	0.2021	0.2021	0.2021	0.2011	0.2014
IGD	**0.0023**	0.0023	0.0024	0.0024	0.0024	0.0024	0.0023
CPF	**260**	259	260	260	260	257	298
PT, sec.	**31**	40	53	66	156	20	24
CPF/PT	**8.5**	6.5	4.9	3.9	1.7	12.9	12.4
FT6 - Zitzler-Deb-Thiele's function N. 4							
LHV	**0.0770**	0.0708	0.0778	0.0780	0.0779	0.0653	0.0669
IGD	**0.0094**	0.0145	0.0154	0.0113	0.0100	0.0100	0.0100
CPF	**926**	58	291	2323	2414	111	133
PT, sec.	**40**	38	57	121	429	20	23
CPF/PT	**23.4**	1.5	5.1	19.2	5.6	5.6	5.8

distribution having the means $\hat{a}$, $\hat{g}$ standard deviations σ, w corresponding to the conditions of extreme traffic with peak loads;

- $\widehat{a}_j\ (w,\ \varsigma)$, $\widehat{g}_j\ (h,\ \upsilon)$ are the arrival intensities and motion speed of the j^{th} agent, $(j \in I \bigcup \tilde{I})$ in the conditions of normal traffic that is random value having the Gaussian distribution with the means w, h and standard deviations ς, υ.

The parameters of distributions define values of arrival intensities and motion speeds corresponding to considered scenarios are presented in Table 2.

Further, to set values of control parameters (e.g., STL's states, signal cycle lengths) at the initial moment t_1, $(t_1 \in T)$ that are to be optimized with the BORCGA-BOPSO, there is suggested to use the distributions with heavy tails, in particular, based on the combination of the LambertW function and the log-normal distribution. That allows us to significantly reduce the dimensionality of initial optimization problem (6) keeping up the adequate of obtained results.

TABLE 2. Parameters of normal distributions for agents.

No.	Parameters		Mean	Std. deviation
Scenario 1 and Scenario 2 in non-peak traffic times				
1	Arrival intensity of agents, (agents/min).	Vehicles	2	0.1
		Pedestrians	1	0.01
2	Velocity of agents, (mi/h).	Vehicles	37.29	3
		Pedestrians	2.8	0.1
Scenario 2 in peak traffic times				
3	Arrival intensity of agents, (agents/min).	Vehicles	4	0.2
		Pedestrians	2	0.02
4	Velocity of agents, (mi/h).	Vehicles	27.96	2
		Pedestrians	3.2	0.05

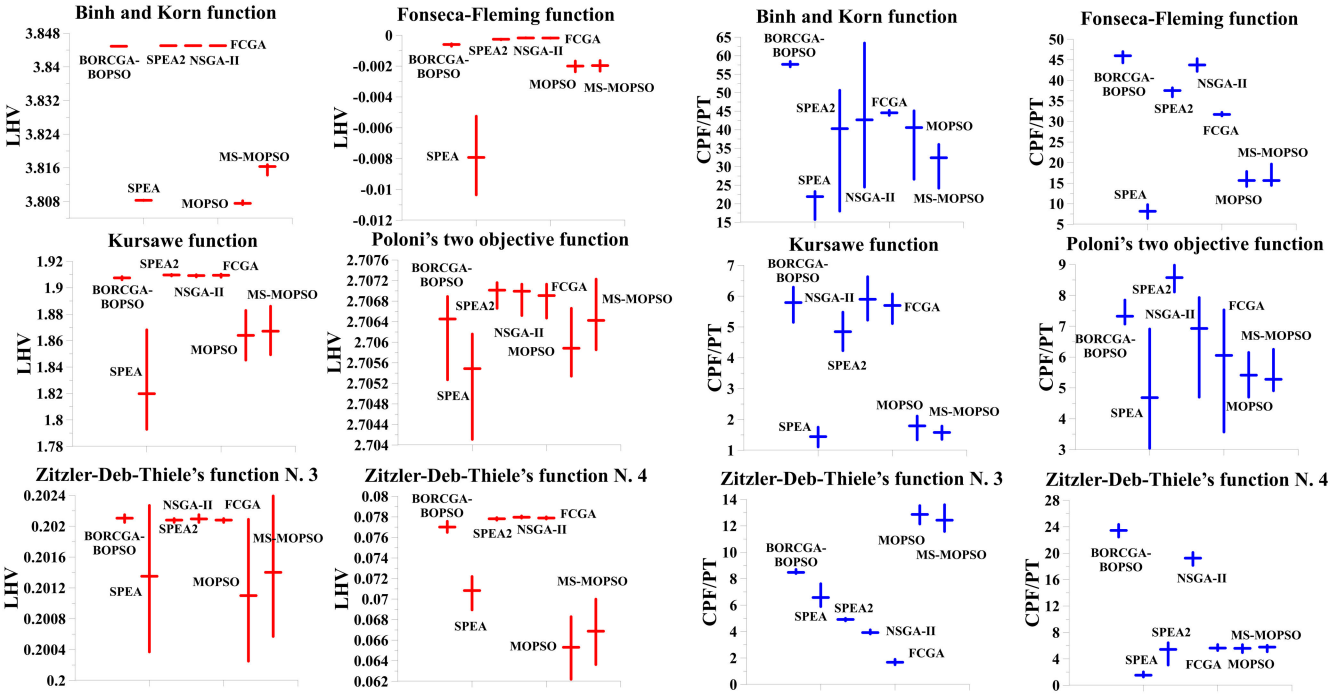

FIGURE 4. Value ranges of and LHV and PT.

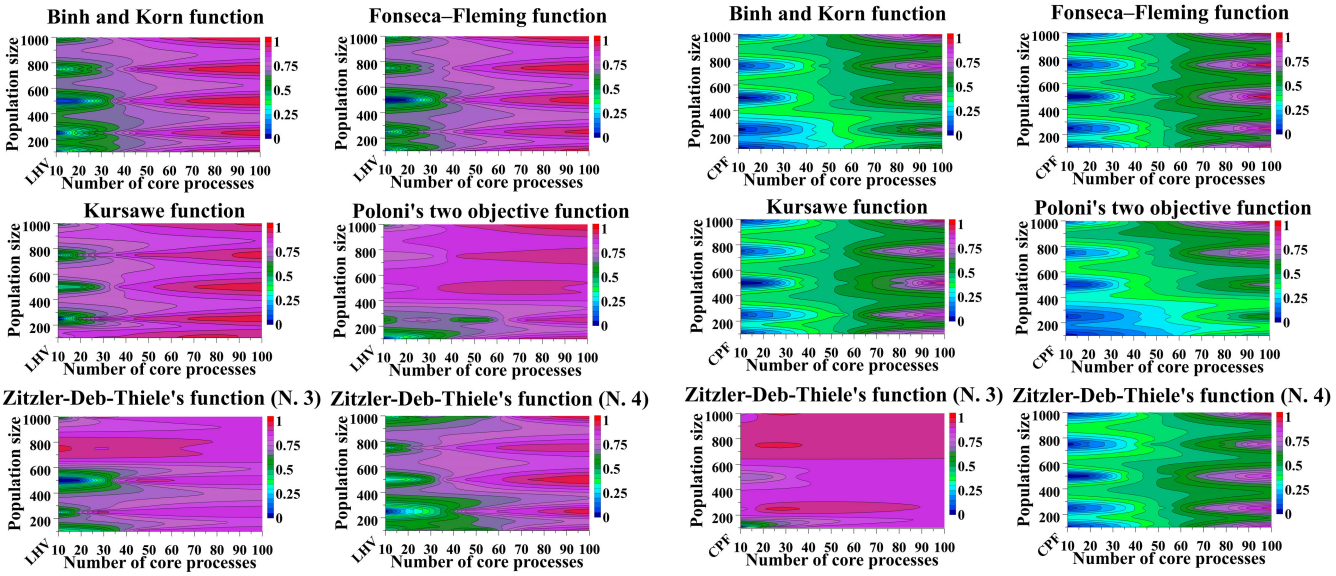

FIGURE 5. Sensitivity tests completed with the BORCGA-BOPSO: dependencies of the normalized values of LHV and CPF on the local population size and the number of core processes, where the best values of performance metrics correspond to 1 and the worst values of performance metrics correspond to 0.

The value of a control parameter charterizing the turn-on or turn-off state of l^{th}- STL, $(l \in L)$ can be given at moment t_1, $(t_1 \in T)$ as follows:

$$\psi_l(t_1) = \lfloor \text{Lambert}W\ (\ln n_l(\mu,\ \eta)) \rfloor\,, \tag{19}$$

where,

- L is the set of STLs' indices;
- Lambert$W$ $(\ln n_l(\mu,\ \eta))$ is a random value having the heavy-tailed distribution [80] generated with the Lambert W function, $\lfloor . \rfloor$ means the whole part of the result;
- $n_l(\mu,\ \eta)$ is a random value having lognormal distribution with parameters $\mu,\ \eta$, where $\mu \in [-1,\ 1]$, $\eta \in (0,\ 1]$.

The values of control parameters characterizing the base values of signal cycle lengths of the l^{th} STL, $(l \in L)$ can be

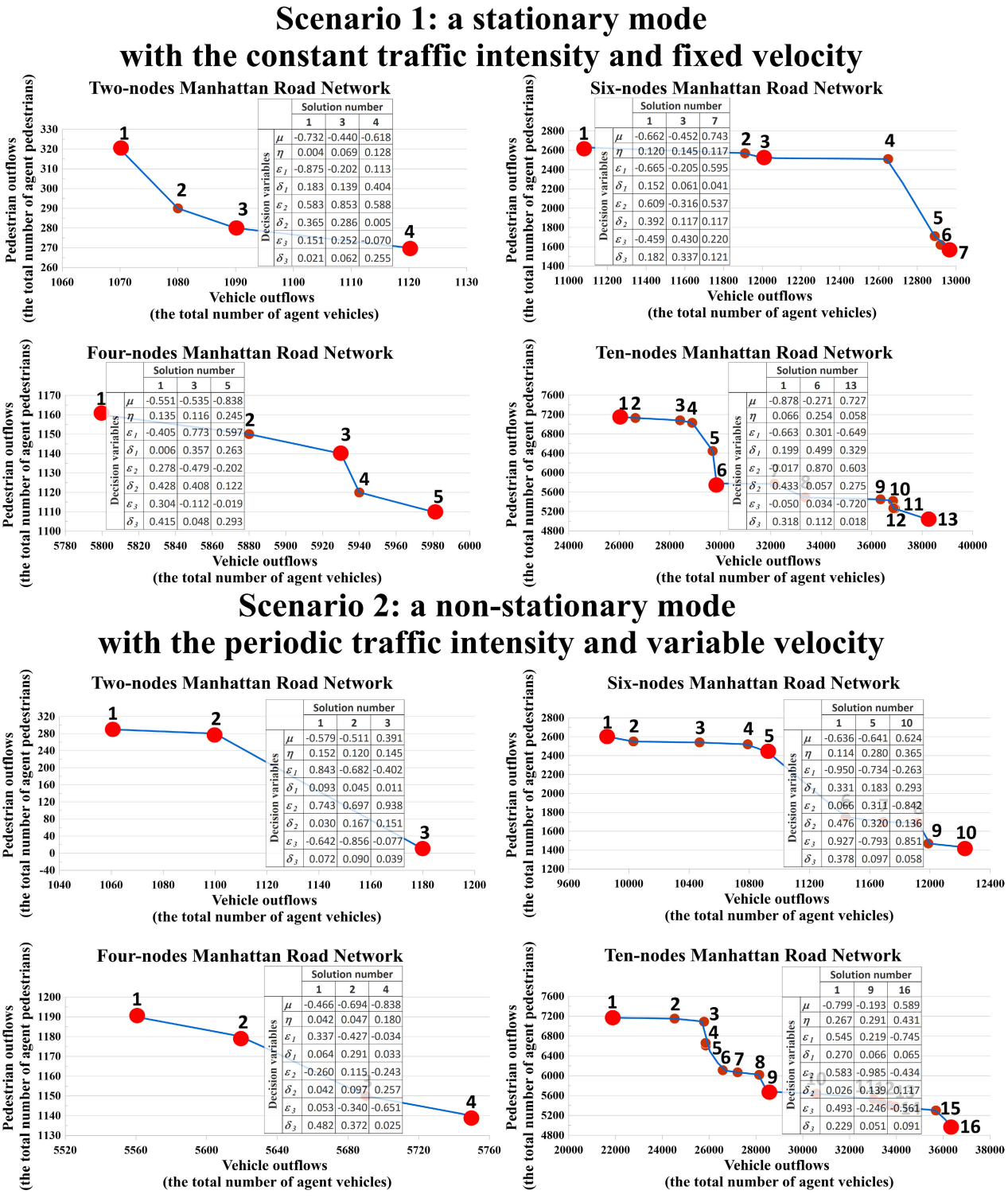

FIGURE 6. The Pareto frontiers computed with the use of the BORCGA-BOPSO for Manhattan road networks.

given at moment t_1, ($t_1 \in T$) with the use the similar way:

$$\tau_{1l}(t_1) = \underline{\tau}_1 + \text{LambertW}\,(\ln m_{1l}(\varepsilon_1,\ \delta_1))\,\bar{\tau}_1, \qquad (20)$$

$$\tau_{2l}(t_1) = \underline{\tau}_2 + \text{LambertW}\,(\ln m_{2l}(\varepsilon_2,\ \delta_2))\,\bar{\tau}_2, \qquad (21)$$

$$\tau_{3l}(t_1) = \underline{\tau}_3 + \text{LambertW}\,(\ln m_{3l}(\varepsilon_3,\ \delta_3))\,\bar{\tau}_3, \qquad (22)$$

where

- $\{\tau_{1l}(t_1),\ \tau_{2l}(t_1),\ \tau_{3l}(t_1)\}$ are signal cycle lengths of the l^{th} STL ($l \in L$) (“red”, “yellow”, “green” signals) given at moment t_1 ($t_1 \in T$);
- $\{\underline{\tau}_1,\ \underline{\tau}_2,\ \underline{\tau}_3\}, \{\bar{\tau}_1,\ \bar{\tau}_2,\ \bar{\tau}_3\}$ are values of lower and upper limits of STLs’ signal cycles lengths;

TABLE 3. Boundary values for STLs' signal cycles lengths.

No.	Parameters		Values
1	Lower limits of STLs signals, sec.	"red"	10
		"yellow"	2
		"green"	10
2	Upper limits of STLs signals, sec.	"red"	110
		"yellow"	4
		"green"	199

- $m_{1l}(\varepsilon_1,\ \delta_1)$, $m_{2l}(\varepsilon_2,\ \delta_2)$, $m_{3l}(\varepsilon_3,\ \delta_3)$ are random values having lognormal distributions with parameters $\{\varepsilon_1,\ \delta_1\}$, $\{\varepsilon_2,\ \delta_2\}$, $\{\varepsilon_3,\ \delta_3\}$, where $\varepsilon_1, \varepsilon_2, \varepsilon_3 \in [-1,\ 1]$, $\delta_1, \delta_2, \delta_3 \in (0,\ 1]$.

The values of lower and upper limits of STLs' signal cycles lengths are presented in Table 3.

In (19)-(22), the use of the Lambert W function is caused by the necessary to nonuniform control of STLs when taking into account probabilistic forming traffic congestions on separate sections of the MRN. Thus, the results of optimization with the BORCGA-BOPSO without considering other characteristics of STLs related to clustering traffic is the set of control parameters: $\{\{\mu,\ \eta\},\ \{\varepsilon_1,\ \delta_1\},\ \{\varepsilon_2,\ \delta_2\},\ \{\varepsilon_3,\ \delta_3\}\}$.

The total number of time moments in the model $|T| = 3600$, sec. The two-lane road width $w = 25$ ft and the distance between the nearest crossroads in simulated road networks $L = 100$ ft.

B. RESULTS OBTAINED

Fig. 6 presents the results of solving biobjective optimization problem as Pareto frontiers computed with the use of the BORCGA-BOPSO for MRNs with different number of nodes and for two scenarios corresponding to the stationary and non-stationary modes of traffic flows.

It is evident from Fig. 6 that the BORCGA-BOPSO is able to form the Pareto frontiers in deferent scenarios and the configuration of MRNs. With the increasing complexity of the MRN and growing the number of nodes, the number of obtained Pareto optimal solutions increase either. Using the STLs in the studied ITS allows keeping up the stability of such solutions and a high level of vehicle and pedestrian output flows in conditions of a non-stationary mode with the periodic traffic intensity and variable velocity. Any particular solution belonging to the Pareto front can be selected among others to analyze the configuration of the MRN related to the appropriate control parameters.

As shown in Fig. 6, three of particular solutions which are the most different in values of objective functions were chosen as the example for each the Pareto front. At the same time, the values of decision variables also change among the different points of the Pareto front.

Fig. 7 shows the results of the sensitivity analysis for the most important control parameters of the ITS based on MRNs with STLs related to the share of switched-off STLs and the green signal cycle length of STLs (under the fixed values of other signals cycle lengths).

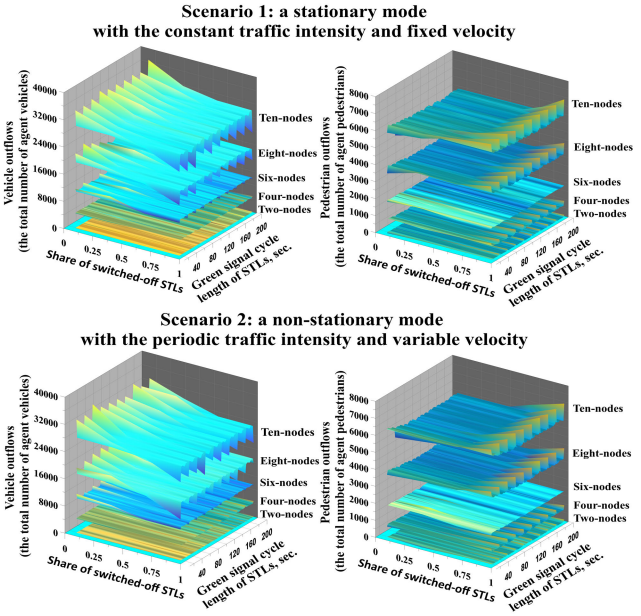

FIGURE 7. Results of a sensitivity analysis for the ITS based on Manhattan road networks with STLs.

As evident from Fig. 7, the vehicle and pedestrian outflows depend on the share of switched-off STLs. The vehicle traffic decreases with the growing of the number of switched-off STLs is due to pedestrians have a priority on uncontrolled crosswalks within the ITS. At the same time, it has a positive influence for pedestrian traffic. Raising the length green signal cycle length of STLs does not lead to a considerable decrease in pedestrian traffic because such STLs are forcibly switched in the prevailing number of pedestrians on controlled crosswalks including the conditions of a non-stationary mode with the periodic traffic intensity and variable velocity. The positive impact of STLs is manifested when the number of MRN's nodes is significant (e.g., eight-nodes, ten-nodes). Such STLs can be switched-off for simple configurations of road networks with the low dimensionality.

In simulated scenarios, the same number of vehicles and pedestrians try to arrive into the MRN with the given intensities and preferred velocities. However, there are situations when some of them do not appear (or appear with a delay) due to queue spillbacks. This can be caused by excessive pedestrian buildups or traffic congestions appearing near entrances to the MRN. Thus, a realistic traffic model is considered here.

In Appendix C are presented the results of the Monte Carlo experiments for MRNs. These histograms illustrate the sensitivity of vehicle and pedestrian outflows regarding the set of control parameters $\{\{\mu,\ \eta\},\ \{\varepsilon_1,\ \delta_1\},\ \{\varepsilon_2,\ \delta_2\},\ \{\varepsilon_3,\ \delta_3\}\}$, which values are updated randomly with use of uniform distributions. The variability of the scenarions obtained confirms the justification of the application of the BORCGA-BOPSO to maximize the output traffic flows.

V. CONCLUSION

In this paper, a new model of the Intelligent Transportation System (ITS) based on Manhattan Road Networks

(MRNs) with Smart Traffic Lights (STLs) is developed. Such STLs use the fuzzy clustering algorithm aggregated with the density-based spatial clustering algorithm (FCA-DBSCAN) to provide an adaptive control of vehicle and pedestrian traffic on crosswalks (**Algorithm 1**). At the same time, the initial values of control parameters of STLs, such as the switched-on and switched-off states and signal cycle lengths are computed as a result of solving the biobjective optimization problem of the ITS.

The ITS has two interconnected objectives: the pedestrian and vehicle traffic outflows, i.e., the total number of pedestrians and vehicles that left the traffic area of the MRN, which should be maximized. For solving such large-scale simulation-based biobjective optimization problem there is suggested a novel parallel hybrid biobjective real-coded genetic algorithm (BORCGA-BOPSO) (**Algorithm 2**). The BORCGA-BOPSO significantly improves the time-efficiency of seeking the Pareto optimal solutions keeping up the approximation quality of the Pareto frontiers in comparison to some well-known multiobjective optimization algorithms (Table 1 and Figs. 3–5). It is provided is due to combined using the Biobjective Real-Coded Genetic Algorithm and the Biobjective Particle Swarm Optimization Algorithm. The test instances used to examine the performance of the BORCGA-BOPSO are presented in Appendix B.

The BORCGA-BOPSO is applied to form the Pareto frontiers for considered biobjective optimization problem in different scenarios, in particular, in a stationary mode and a non-stationary mode with the periodic traffic intensity and variable velocity (Fig. 6). The results of the Monte Carlo experiments (Appendix C) and the sensitivity analysis (Fig. 7) confirm the ability to improve both vehicle and pedestrian flows at various road network configurations of MRNs and using STLs.

APPENDIX A
NOTATIONS INTRODUCED

The following notations are used in the transportation model.

- T is the set of time moments (in minutes), $|T|$ is the total number of time moments; $t_1 \in T, t_{|T|} \in T$ is the start and end moments; $t_k \in T, k = 1, \ldots, |T|$ is all moments of time;
- $I = \{i_1, i_2, \ldots, i_{|I|}\}$ is the set of indices of agent pedestrians, where $|I|$ is the total number of pedestrians;
- $\tilde{I} = \{\tilde{i}_1, \tilde{i}_2, \ldots, \tilde{i}_{\left|\tilde{I}\right|}\}$ is the set of indices of agent vehicles, where $\left|\tilde{I}\right|$ is the total number of vehicles;
- $L = \{l_1, l_2, \ldots, l_{|L|}\}$ is the set of STLs' indices, where $|L|$ is the total number of STLs;
- $\left\{s_l^*(t_k) \in \{1, 2, 3\}, r_l^*\right\}, l \in L, t_k \in T$ is the state of the l^{th} STL at moment t_k, which determines the current signal of the smart traffic light (1 is a "red" signal, 2 is a "yellow" signal, and 3 is a "green" signal, prohibiting, warning and allowing the movement of vehicles, respectively), as well as its action radius;
- $r_i(t_k), i \in I, t_k \in T$ is the radius of personal space of the i^{th} agent pedestrian at moment t_k, which value equals to

$$r_i(t_k) = \begin{cases} r, & \text{if } \rho_i(t_k) = 1, \\ \frac{r}{(\rho_i(t_k))^\eta}, & \text{if } 1 < \rho_i(t_k) < \bar{\rho}, \\ \frac{\gamma r}{(\rho_i(t_k))^\eta}, & \text{if } \bar{\rho} < \rho_i(t_k) < \bar{\bar{\rho}}, \\ 0, & \text{if } \bar{\bar{\rho}} \le \rho_i(t_k), \end{cases} \tag{23}$$

where, r is the base value of the radius of the personal space of the agent pedestrian that is set at the initial moment $t_1 \in T$; $\rho_i(t_k)$ is the density of the environment that surrounds the i^{th}-agent pedestrian, $(i \in I)$; $0 \le \eta \le 1$ and $\gamma > 1$ are coefficients with given values that determine the agent's response to changes in the density of the surrounding environment; $\bar{\rho}$, $\bar{\bar{\rho}}$ are threshold coefficients of the density of the pedestrian flow, which determine the conditions for the occurrence of a state of panic, "crush", etc.;

- $\tilde{r}_{\tilde{i}}(t_k), \tilde{i} \in \tilde{I}, t_k \in T$ is the radius of the personal space of the $\tilde{i}^{th}$ agent vehicle at moment t_k, the value of which is computed on the basis of assessing the density of the traffic flow considering the influence of the "stop-and-go wave effect" (Fig. 2a) and it is equal to

$$\tilde{r}_{\tilde{i}}(t_k) = \begin{cases} \hat{r}_{\tilde{i}}(t_{k-1}), & \text{if } \tilde{\rho}_{\tilde{i}}(t_k) = 1, \\ \frac{\hat{r}_{\tilde{i}}(t_{k-1})}{\left(\rho_{\tilde{i}}(t_k)\right)^\eta}, & \text{if } 1 < \tilde{\rho}_{\tilde{i}}(t_k) < \bar{\bar{\rho}}, \\ \frac{\gamma \hat{r}_{\tilde{i}}(t_{k-1})}{\left(\rho_{\tilde{i}}(t_k)\right)^\eta}, & \text{if } \bar{\rho} < \rho_{\tilde{i}}(t_k) < \bar{\bar{\rho}}, \\ 0, & \text{if } \bar{\bar{\rho}} \le \rho_{\tilde{i}}(t_k), \end{cases} \tag{24}$$

$$\hat{r}_{\tilde{i}}(t_k) = \begin{cases} r', & \text{if } t_k = t_1, \\ \tilde{r}_{\tilde{i}}(t_{k-1}), & \text{if XVIII is true}, \\ \varpi \hat{r}_{\xi}(t_{k-1}), & \text{if XIX is true}, \end{cases} \tag{25}$$

where

XVIII. $d_{\tilde{i}\xi}(t_{k-1}) > \left(\tilde{r}_{\tilde{i}}(t_{k-1}) + \tilde{r}_{\xi}(t_{k-1})\right)$, *which means the agent vehicle does not interact with another agent located ahead and stopped at moment* t_k, $(t_k \in T)$,

XIX. $d_{\tilde{i}\xi}(t_{k-1}) \le \left(\tilde{r}_{\tilde{i}}(t_{k-1}) + \tilde{r}_{\xi}(t_{k-1})\right)$, *which means the agent vehicle interacts with another agent located ahead and stopped at moment* t_k, $(t_k \in T)$.

Here, r' is the base value of the radius of the personal space of the agent vehicle that is set at the initial moment $t_1 \in T$; $\rho_{\tilde{i}}(t_k)$ is the density of the environment that surrounds the $\tilde{i}^{th}$- agent vehicle, $(\tilde{i} \in \tilde{I})$; $0 \le \eta \le 1$ and $\gamma, \varpi > 1$ are coefficients with given values that determine the agent's response to changes in environmental characteristics; $d_{\tilde{i}\xi}(t_k)$ is the distance between the $\tilde{i}^{th}$ agent vehicle, $(\tilde{i} \in \tilde{I})$ and the ξ^{th} vehicle, $(\xi \in \tilde{I})$ located ahead and stopped at moment t_k, when $d_{\tilde{i}\xi} > \left(\tilde{r}_{\tilde{i}}(t_{k-1}) + \tilde{r}_{\xi}(t_{k-1})\right)$, then this means the absence of such a vehicle;

- $\{\underline{x}, \underline{y}\}, \quad \{\bar{x}, \bar{y}\}$ are given coordinates of the lower left and upper right corners of the MRN space;

TABLE 4. Test instances for BORCGA-BOPSO.

Title	Problem statement (objectives to be minimized)	Variable bounds
FT1 – Binh and Korn function [73]	$\begin{cases} f_1 = 4x^2 + 4y^2 \\ f_2 = (x-5)^2 + (y-5)^2 \end{cases}$ s.t. $\begin{cases} g_1 = (x-5)^2 + y^2 \le 25 \\ g_2 = (x-8)^2 + (y+3)^2 \ge 7.7 \end{cases}$	$0 \le x \le 5$ $0 \le y \le 3$
FT2 – Fonseca-Fleming function [74]	$\begin{cases} f_1 = 1 - \exp\left(-\sum_{j=1}^{n}\left(x_j - \frac{1}{\sqrt{n}}\right)^2\right) \\ f_2 = 1 - \exp\left(-\sum_{j=1}^{n}\left(x_j + \frac{1}{\sqrt{n}}\right)^2\right) \end{cases}$	$-4 \le x_j \le 4$ $1 \le j \le n$
FT3 –Kursawe function [75]	$\begin{cases} f_1 = \sum_{j=1}^{2}(-10)\exp\left(-0.2\sqrt{x_j^2 + x_{j+1}^2}\right) \\ f_2 = \sum_{j=1}^{3}\left(\lvert x_j\rvert^{0.8} + 5x_j^3\right) \end{cases}$	$-5 \le x_j \le 5$ $1 \le j \le 3$
FT4 – Poloni's two objective function [76]	$\begin{cases} f_1 = 1 + (A_1 - B_1)^2 + (A_2 - B_2)^2 \\ f_2 = (x+3)^2 + (y+1)^2 \end{cases}$ Where $\begin{cases} A_1 = 0.5\sin 1 - 2\cos 1 + \\ \sin 2 - 1.5\cos 2 \\ A_2 = 1.5\sin 1 - \cos 1 + \\ 2\sin 2 - 0.5\cos 2 \\ B_1 = 0.5\sin x - 2\cos x + \\ \sin y - 1.5\cos y \\ B_2 = 1.5\sin x - \cos x + \\ 2\sin y - 0.5\cos y \end{cases}$	$-\pi \le x \le \pi$ $-\pi \le y \le \pi$
FT5 – Zitzler-Deb-Thiele's function N. 3 [77]	$\begin{cases} f_1 = x_1 \\ f_2 = gh \end{cases}$ Where $\begin{cases} g = 1 + \frac{9}{29}\sum_{j=2}^{30} x_j \\ h = 1 - \sqrt{\frac{f_1}{g}} - \left(\frac{f_1}{g}\right)\sin(10\pi f_1) \end{cases}$	$0 \le x_j \le 1$ $1 \le j \le 30$
FT6 – Zitzler-Deb-Thiele's function N. 4 [77]	$\begin{cases} f_1 = x_1 \\ f_2 = gh \end{cases}$ Where $\begin{cases} g = 91 + \sum_{j=2}^{10}\left({x_j}^2 - 10\cos\left(4\pi x_j\right)\right) \\ h = 1 - \sqrt{\frac{f_1}{g}} \end{cases}$	$0 \le x_j \le 1$ $-5 \le j \le 5$ $2 \le j \le 10$

- $\{x_i(t_k),\ y_i(t_k)\}$, $\{\tilde{x}_{\tilde{i}}(t_k),\ \tilde{y}_{\tilde{i}}(t_k)\}$ are coordinates of the i^{th} agent pedestrian, $(i \in I)$ and the $\tilde{i}^{th}$ agent vehicle, $(\tilde{i} \in \tilde{I})$ at moment t_k, $(t_k \in T)$;
- $s_j(t_k) \in \{1,\ 2,\ 3,\ 4\}$ is the parameter that specifies the possible states of the j^{th} agent, $(j \in I \bigcup \tilde{I})$ at moment t_k, $(t_k \in T)$: $s_j(t_k) = 1$ means the target movement

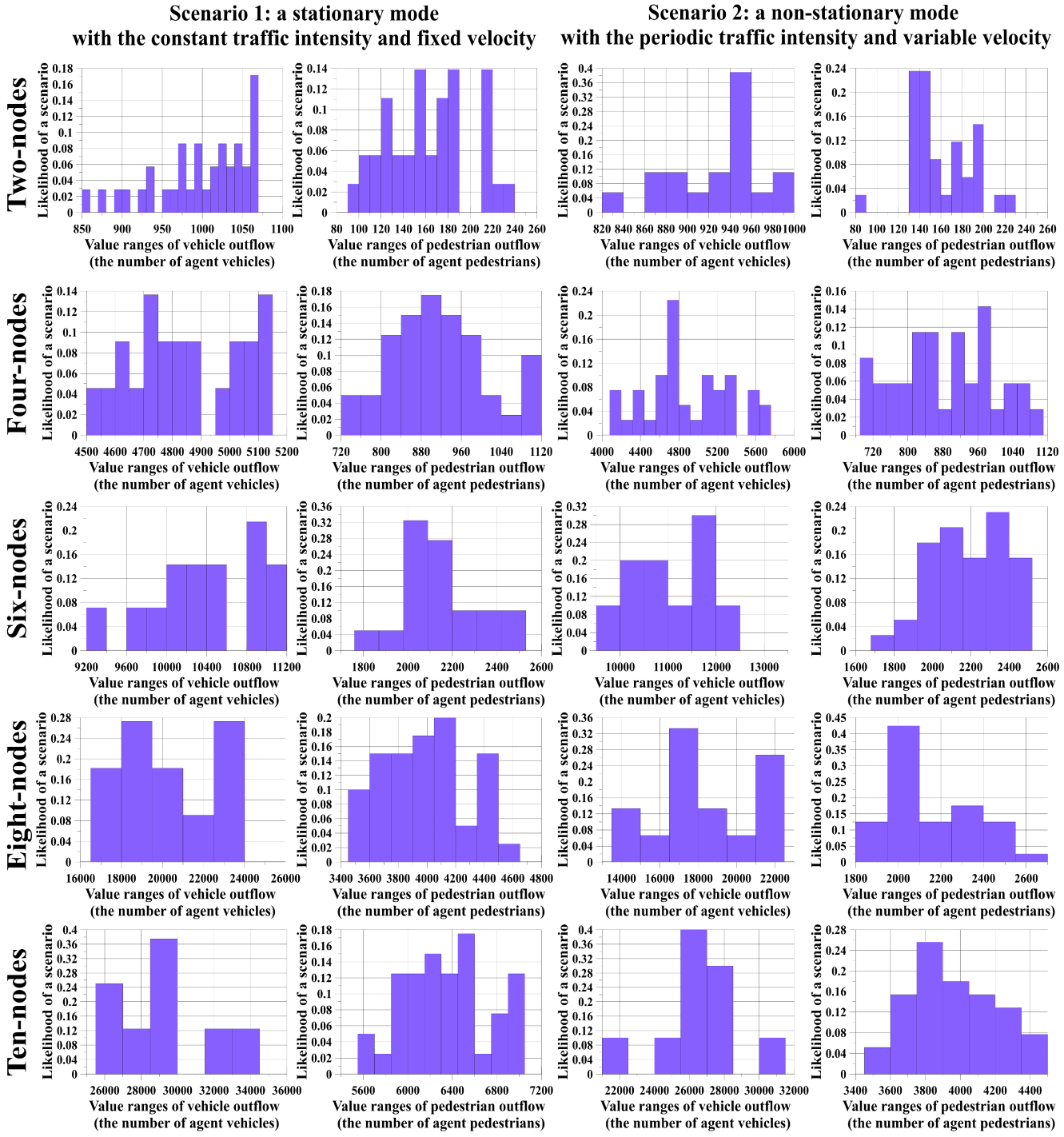

FIGURE 8. Results of the Monte Carlo experiments for Manhattan road networks.

towards the "left-to-right" direction ("*E-W*"), $s_j(t_k) = 2$ means the target movement towards the "right-to-left" direction ("*W-E*"), $s_j(t_k) = 3$ means the target movement towards the "bottom-up" direction ("*S-N*"), and $s_j(t_k) = 4$ means the target movement towards the "top-down" direction ("*N-S*");

- $\delta_j(t_k)$ is the sign that specifies the direction of changes in coordinates of the j^{th}-agent, $(j \in I \bigcup \tilde{I})$ depending on its state at moment t_k, $(t_k \in T)$:

$$\delta_j(t_k) = \begin{cases} 1, & \text{if } s_j(t_{k-1}) \in \{1,\ 3\}, \\ -1, & \text{if } s_j(t_{k-1}) \in \{2,\ 4\}. \end{cases} \tag{26}$$

- $d^*_{jl}(t_k)$ is the distance between the j^{th} agent, $(j \in I \bigcup \tilde{I})$ and the nearest l^{th} STL, $(l \in L)$, respectively, at moment t_k, $(t_k \in T)$;

- $\tilde{d}_{j\xi}(t_k)$ is the distance between the j^{th} agent, $(j \in I \bigcup \tilde{I})$ and the nearest ξ^{th}-agent, $(\xi \in I \bigcup \tilde{I})$;
- $g_j(h,\ \delta h)$ is the motion speed of the j^{th} agent, $(j \in I \bigcup \tilde{I})$ that is a random value having the Gaussian distribution with the mean h and the standard deviation δh, respectively;
- $\{p_j(0,\ 1),\ \underline{p}\}$ is a random value distributed uniformly in the range of $(0,\ 1)$, that specifies the probability of strict observance of traffic rules by the j^{th} agent, $(j \in I \bigcup \tilde{I})$ and the threshold level of compliance with traffic rules, respectively;
- $\mu_j(t_k) \in \{0,\ 1\}$ is the parameter that allows movement for the j^{th}-agent, $(j \in I \bigcup \tilde{I})$ in action areas of STLs at moment t_k $(t_k \in T)$: $\mu_j(t_k) = 0$ means movement is prohibited, $\mu_j(t_k) = 1$ means movement is allowed:

$$\mu_j(t_k) = \begin{cases} 0, \text{ if XX is true,} \\ 1, \text{ if XXI is true,} \end{cases} \tag{27}$$

where

XX. $(d^*_{jl}(t_{k-1}) \le r^*_l$ *and* $s^*_l(t_{k-1}) = 3$ *and* $p_j(t_{k-1}) \ge \underline{p}$ *for* $j \in I$*) or* $(d^*_{jl}(t_{k-1}) \le r^*_l$ *and* $s^*_l(t_{k-1}) = 1$ *and* $p_j(t_{k-1}) \ge \underline{p}$ *for* $j \in \tilde{I}$*), which means the agent complying with the traffic rules is in the area of the prohibition signal of a traffic light,*

XXI. $(d^*_{jl}(t_{k-1}) \le r^*_l$ *and* $s^*_l(t_{k-1}) = 1$ *for* $j \in I$*) or* $(d^*_{jl}(t_{k-1}) \le r^*_l$ *and* $s^*_l(t_{k-1}) = 3$ *for* $j \in \tilde{I}$*) or* $(d^*_{jl}(t_{k-1}) > r^*_l$ *for any* $l \in L$*), which means the agent is in the action zone of the permissive traffic light signal, or outside the coverage area of any traffic light.*

- κ is the "rebound" coefficient due to the desire of agents to avoid a collision;
- $\hat{l}$ is the distance between each pair of nearest crossroads of the road network, which specifies the dimension of one node of the MRN (Fig. 1);
- λ is the coefficient that specifies the ratio of the real and virtual model time scales considering the space's dimensionality of the MRN.
- $\beta_{j\xi}(t_{k-1})$ is the offset angle of the j^{th}agent, $(j \in I \bigcup \tilde{I})$ to detour the nearest ξ^{th}- agent, $(\xi \in I \bigcup \tilde{I},\ j \ne \xi)$ at moment t_{k-1}, $(t_{k-1} \in T)$:

$$\beta_{j\xi}(t_{k-1}) = \frac{\pi}{4} + \left| \arctan \frac{\begin{array}{l} y_\xi(t_{k-1}) - y_j(t_{k-1}) \\ + \left(r_\xi(t_{k-1}) + r_j(t_{k-1})\right) \\ \times \sin\frac{\pi}{4} \end{array}}{\begin{array}{l} x_\xi(t_{k-1}) - x_j(t_{k-1}) \\ + \left(r_\xi(t_{k-1}) + r_j(t_{k-1})\right) \\ \times \cos\frac{\pi}{4} \end{array}} \right|, \tag{28}$$

- $\gamma_{j\xi}(t_{k-1})$ is the rebound angle of the j^{th}agent, $(j \in I \bigcup \tilde{I})$ to avoid the nearest ξ^{th} agent, $(\xi \in I \bigcup \tilde{I},\ j \ne \xi)$ at moment t_{k-1}, $(t_{k-1} \in T)$:

$$\gamma_{j\xi}(t_{k-1}) = \pi + \left| \arctan \frac{y_\xi(t_{k-1}) - y_j(t_{k-1})}{x_\xi(t_{k-1}) - x_j(t_{k-1})} \right|. \tag{29}$$

The model has the following set of control parameters:

- $\psi_l(t_k) \in \{0,\ 1\}, l \in L$ is the set of STL's states at moment t_k, $(t_k \in T)$: $\psi_l(t_k) = 0$ means the l^{th} STL is switched-off, $\psi_l(t_k) = 1$ means the l^{th} STL is switched-on;
- $\{\tau_{1l}(t_k), \tau_{2l}(t_k), \tau_{3l}(t_k)\}, l \in L$ are signal cycle lengths of the l^{th} STL ("red", "yellow", "green" signals) given for moment t_k, $(t_k \in T)$;
- $\{|C_l|,\ \varphi_l,\ \eta_l\},\ l \in L$ are main parameters of the adaptive algorithm (FCA-DBSCAN) used to explore the structure of traffic flows and control of STLs, where $|C_l|$ is the total number of clusters in the fuzzy clustering algorithm used by the l^{th} STL, φ_l is the threshold ratio between the number of vehicles in the nearest cluster and the number of pedestrians located close to crosswalk controlled by the l^{th} STL to switch signals and balance the speed of traffic flows, η_l is the radius of monitoring area covered by the l^{th} STL.

APPENDIX B
TEST INSTANCES

See Table 4.

APPENDIX C
MONTE CARLO EXPERIMENTS FOR MANHATTAN ROAD NETWORKS

See Figure 8.

REFERENCES

[1] T. Shen, K. Hua, and J. Liu, "Optimized public parking location modelling for green intelligent transportation system using genetic algorithms," *IEEE Access*, vol. 7, pp. 176870–176883, 2019.
[2] S. Zhang, C. Lu, S. Jiang, L. Shan, and N. N. Xiong, "An unmanned intelligent transportation scheduling system for open-pit mine vehicles based on 5G and big data," *IEEE Access*, vol. 8, pp. 135524–135539, 2020.
[3] Y. Yang, Q. Zhou, and K. Chen, "Multiagent-based modeling and simulation of a coal multimodal transport system," *IEEE Access*, vol. 10, pp. 65873–65885, 2022.
[4] W. Yao, "A multi-objective collaborative planning strategy for integrated power distribution and electric vehicle charging systems," *IEEE Trans. Power Syst.*, vol. 29, no. 4, pp. 1811–1821, Jul. 2014.
[5] A. S. Akopov, L. A. Beklaryan, and M. Thakur, "Improvement of maneuverability within a multiagent fuzzy transportation system with the use of parallel biobjective real-coded genetic algorithm," *IEEE Trans. Intell. Transp. Syst.*, vol. 23, no. 8, pp. 12648–12664, Aug. 2022.
[6] A. S. Akopov, L. A. Beklaryan, and A. L. Beklaryan, "Simulation-based optimisation for autonomous transportation systems using a parallel real-coded genetic algorithm with scalable nonuniform mutation," *Cybern. Inf. Technol.*, vol. 21, no. 3, pp. 127–144, Sep. 2021.
[7] C. Tang, S. Xia, C. Zhu, and X. Wei, "Phase timing optimization for smart traffic control based on fog computing," *IEEE Access*, vol. 7, pp. 84217–84228, 2019.
[8] A. M. Turky, M. S. Ahmad, M. Z. M. Yusoff, and B. T. Hammad, "Using genetic algorithm for traffic light control system with a pedestrian crossing," in *Rough Sets and Knowledge Technology*, vol. 5589. Berlin, Germany: Springer, 2009.
[9] H. Dezani, N. Marranghello, and F. Damiani, "Genetic algorithm-based traffic lights timing optimization and routes definition using Petri net model of urban traffic flow," *IFAC Proc. Volumes*, vol. 47, no. 3, pp. 11326–11331, 2014.
[10] I. M. Albatish and S. S. Abu-Naser, "Modeling and controlling smart traffic light system using a rule based system," in *Proc. Int. Conf. Promising Electron. Technol. (ICPET)*, Oct. 2019, pp. 55–60.

[11] A. Kanungo, A. Sharma, and C. Singla, "Smart traffic lights switching and traffic density calculation using video processing," in *Proc. Recent Adv. Eng. Comput. Sci. (RAECS)*, Chandigarh, India, Mar. 2014, pp. 1–6.

[12] S. S. S. M. Qadri, M. A. Gökçe, and E. Öner, "State-of-art review of traffic signal control methods: Challenges and opportunities," *Eur. Transp. Res. Rev.*, vol. 12, no. 1, Dec. 2020, Art. no. 55.

[13] M. Bando, K. Hasebe, A. Nakayama, A. Shibata, and Y. Sugiyama, "Dynamical model of traffic congestion and numerical simulation," *Phys. Rev. E, Stat. Phys. Plasmas Fluids Relat. Interdiscip. Top.*, vol. 51, no. 2, pp. 1035–1042, Feb. 1995.

[14] D. Helbing, "Traffic and related self-driven many-particle systems," *Rev. Modern Phys.*, vol. 73, no. 4, pp. 1067–1141, Dec. 2001.

[15] J. A. Laval and L. Leclercq, "A mechanism to describe the formation and propagation of stop-and-go waves in congested freeway traffic," *Phil. Trans. Roy. Soc. A, Math., Phys. Eng. Sci.*, vol. 368, no. 1928, pp. 4519–4541, Oct. 2010.

[16] A. Ghiasi, X. Li, and J. Ma, "A mixed traffic speed harmonization model with connected autonomous vehicles," *Transp. Res. C, Emerg. Technol.*, vol. 104, pp. 210–233, Jul. 2019.

[17] J. Luo, Y.-S. Huang, and Y.-S. Weng, "Design of variable traffic light control systems for preventing two-way grid network traffic jams using timed Petri nets," *IEEE Trans. Intell. Transp. Syst.*, vol. 21, no. 7, pp. 3117–3127, Jul. 2020.

[18] A. Vogel, I. Oremovic, R. Šimic, and E. Ivanjko, "Improving traffic light control by means of fuzzy logic," in *Proc. Int. Symp. ELMAR*, Zadar, Croatia, Sep. 2018, pp. 51–56.

[19] S. S. Sarma, K. Sinha, C. Sub-r-pa, G. Chakraborty, and B. P. Sinha, "Optimal distribution of traffic in Manhattan road networks for minimizing routing-time," *IEEE Trans. Intell. Transp. Syst.*, vol. 22, no. 11, pp. 6799–6820, Nov. 2021.

[20] O. Tayan and D. Harle, "Traffic regulation and control in the Manhattan street network," in *Networking* (Lecture Notes in Computer Science), vol. 3042. Berlin, Germany: Springer, 2004.

[21] P. Heywood, P. Richmond, and S. Maddock, "Road network simulation using FLAME GPU," in *Proc. Euro-Par Parallel Process. Workshops Euro-Par*, vol. 9523. Cham, Switzerland: Springer, 2015, pp. 430–441.

[22] D. Helbing and P. Molnár, "Social force model for pedestrian dynamics," *Phys. Rev. E, Stat. Phys. Plasmas Fluids Relat. Interdiscip. Top.*, vol. 51, no. 5, pp. 4282–4286, May 1995.

[23] G. Antonini, M. Bierlaire, and M. Weber, "Discrete choice models of pedestrian walking behavior," *Transp. Res. B, Methodol.*, vol. 40, no. 8, pp. 667–687, 2006.

[24] A. S. Akopov and L. A. Beklaryan, "An agent model of crowd behavior in emergencies," *Autom. Remote Control*, vol. 76, no. 10, pp. 1817–1827, Oct. 2015.

[25] R. Herman and I. Prigogine, "A two-fluid approach to town traffic," *Science*, vol. 204, no. 4389, pp. 148–151, Apr. 1979.

[26] D. Helbing and M. Treiber, "Numerical simulation of macroscopic traffic equations," *Comput. Sci. Eng.*, vol. 1, no. 5, pp. 89–98, 1999.

[27] Z. Wei, Y. Hong, and D. Wang, "The phase diagram and the pathway of phase transitions for traffic flow in a circular one-lane roadway," *Phys. A, Stat. Mech. Appl.*, vol. 388, no. 8, pp. 1665–1672, Apr. 2009.

[28] A. Kotsialos, M. Papageorgiou, C. Diakaki, Y. Pavlis, and F. Middelham, "Traffic flow modeling of large-scale motorway networks using the macroscopic modeling tool METANET," *IEEE Trans. Intell. Transp. Syst.*, vol. 3, no. 4, pp. 282–292, Dec. 2002.

[29] Y. Yuan, J. W. C. van Lint, R. E. Wilson, F. van Wageningen-Kessels, and S. P. Hoogendoorn, "Real-time Lagrangian traffic state estimator for freeways," *IEEE Trans. Intell. Transp. Syst.*, vol. 13, no. 1, pp. 59–70, Mar. 2012.

[30] N. Geroliminis, J. Haddad, and M. Ramezani, "Optimal perimeter control for two urban regions with macroscopic fundamental diagrams: A model predictive approach," *IEEE Trans. Intell. Transp. Syst.*, vol. 14, no. 1, pp. 348–359, Mar. 2013.

[31] Z. H. Khan and T. A. Gulliver, "A macroscopic traffic model for traffic flow harmonization," *Eur. Transp. Res. Rev.*, vol. 10, no. 2, Jun. 2018, Art. no. 30.

[32] K. Li and P. Ioannou, "Modeling of traffic flow of automated vehicles," *IEEE Trans. Intell. Transp. Syst.*, vol. 5, no. 2, pp. 99–113, Jun. 2004.

[33] X. Chen, L. Li, and Y. Zhang, "A Markov model for headway/spacing distribution of road traffic," *IEEE Trans. Intell. Transp. Syst.*, vol. 11, no. 4, pp. 773–785, Dec. 2010.

[34] F. Kessels, "Mesoscopic models," in *Traffic Flow Modelling*. Cham, Switzerland: Springer, 2019, pp. 99–106.

[35] F. D. Souza, O. Verbas, and J. Auld, "Mesoscopic traffic flow model for agent-based simulation," *Proc. Comput. Sci.*, vol. 151, pp. 858–863, Jan. 2019.

[36] V. A. Vu and G. Tan, "A framework for mesoscopic traffic simulation in GPU," *IEEE Trans. Parallel Distrib. Syst.*, vol. 30, no. 8, pp. 1691–1703, Aug. 2019.

[37] M. Treiber, A. Hennecke, and D. Helbing, "Congested traffic states in empirical observations and microscopic simulations," *Phys. Rev. E, Stat. Phys. Plasmas Fluids Relat. Interdiscip. Top.*, vol. 62, no. 2, pp. 1805–1824, Aug. 2000.

[38] S. Panwai and H. Dia, "Comparative evaluation of microscopic car-following behavior," *IEEE Trans. Intell. Transp. Syst.*, vol. 6, no. 3, pp. 314–325, Sep. 2005.

[39] J. Nguyen, S. T. Powers, N. Urquhart, T. Farrenkopf, and M. Guckert, "An overview of agent-based traffic simulators," *Transp. Res. Interdiscipl. Perspect.*, vol. 12, Dec. 2021, Art. no. 100486.

[40] S. Plakolb and N. Strelkovskii, "Applicability of the future state maximization paradigm to agent-based modeling: A case study on the emergence of socially sub-optimal mobility behavior," *Systems*, vol. 11, no. 2, p. 105, Feb. 2023.

[41] A. L. Beklaryan, L. A. Beklaryan, and A. S. Akopov, "Simulation model of an intelligent transportation system for the 'smart city' with adaptive control of traffic lights based on fuzzy clustering," *Bus. Informat.*, vol. 17, no. 3, pp. 70–86, 2023.

[42] J. C. Bezdek, "Cluster validity with fuzzy sets," *J. Cybern.*, vol. 3, no. 3, pp. 58–73, Jan. 1973.

[43] M. Ester, H. P. Kriegel, and X. Xu, "A density-based algorithm for discovering clusters in large spatial databases with noise," in *Proc. 2nd Int. Conf. Knowl. Discovery Data Mining*, vol. 6, 1996, pp. 226–231.

[44] J. Kennedy and R. Eberhart, "Particle swarm optimization," in *Proc. IEEE ICNN*, vol. 4, Nov./Dec. 1995, pp. 1942–1948.

[45] R. Eberhart and J. Kennedy, "A new optimizer using particle swarm theory," in *Proc. MHS. Proc. 6th Int. Symp. Micro Mach. Human Sci.*, Oct. 1995, pp. 39–43.

[46] Bharti, P. Redhu, and K. Kumar, "Short-term traffic flow prediction based on optimized deep learning neural network: PSO-Bi-LSTM," *Phys. A, Stat. Mech. Appl.*, vol. 625, Sep. 2023, Art. no. 129001.

[47] C. A. Coello Coello and M. S. Lechuga, "MOPSO: A proposal for multiple objective particle swarm optimization," in *Proc. Congr. Evol. Comput. (CEC)*, May 2002, pp. 1051–1056.

[48] X. Hu and R. Eberhart, "Multiobjective optimization using dynamic neighborhood particle swarm optimization," in *Proc. Congr. Evol. Comput. (CEC)*, May 2002, pp. 1677–1681.

[49] G. G. Yen and W. F. Leong, "Dynamic multiple swarms in multiobjective particle swarm optimization," *IEEE Trans. Syst., Man, Cybern. A, Syst. Humans*, vol. 39, no. 4, pp. 890–911, Jul. 2009.

[50] M. Z. B. Mohd Zain, J. Kanesan, J. H. Chuah, S. Dhanapal, and G. Kendall, "A multi-objective particle swarm optimization algorithm based on dynamic boundary search for constrained optimization," *Appl. Soft Comput.*, vol. 70, pp. 680–700, Sep. 2018.

[51] A. de Campos, A. T. R. Pozo, and E. P. Duarte, "Parallel multi-swarm PSO strategies for solving many objective optimization problems," *J. Parallel Distrib. Comput.*, vol. 126, pp. 13–33, Apr. 2019.

[52] V. Trivedi, P. Varshney, and M. Ramteke, "A simplified multi-objective particle swarm optimization algorithm," *Swarm Intell.*, vol. 14, no. 2, pp. 83–116, Jun. 2020.

[53] T. M. Shami, A. A. El-Saleh, M. Alswaitti, Q. Al-Tashi, M. A. Summakieh, and S. Mirjalili, "Particle swarm optimization: A comprehensive survey," *IEEE Access*, vol. 10, pp. 10031–10061, 2022.

[54] J. H. Holland, *Adaptation in Natural and Artificial Systems*. Cambridge, MA, USA: MIT Press, 1975.

[55] D. E. Goldberg, *Genetic Algorithms in Search, Optimization and Machine Learning*, 1st ed. Reading, MA, USA: Addison-Wesley, 1989.

[56] F. Herrera, M. Lozano, and J. L. Verdegay, "Tackling real-coded genetic algorithms: Operators and tools for behavioural analysis," *Artif. Intell. Rev.*, vol. 12, no. 4, pp. 265–319, 1998.

[57] A. Kumar and K. Deb, "Real-coded genetic algorithms with simulated binary crossover: Studies on multimodal and multiobjective problems," *Complex Syst.*, vol. 9, pp. 431–454, Sep. 1995.

[58] K. Deep and M. Thakur, "A new crossover operator for real coded genetic algorithms," *Appl. Math. Comput.*, vol. 188, no. 1, pp. 895–911, May 2007.

[59] K. Deep and M. Thakur, "A new mutation operator for real coded genetic algorithms," *Appl. Math. Comput.*, vol. 193, no. 1, pp. 211–230, Oct. 2007.
[60] A. S. Akopov, L. A. Beklaryan, M. Thakur, and B. D. Verma, "Parallel multi-agent real-coded genetic algorithm for large-scale black-box single-objective optimisation," *Knowl.-Based Syst.*, vol. 174, pp. 103–122, Jun. 2019.
[61] A. D. Voronkov and S. A. K. Diane, "Continuous genetic algorithm for grasping an object of a priori unknown shape by a robotic manipulator," *Russian Technol. J.*, vol. 11, no. 1, pp. 18–30, Feb. 2023.
[62] E. Zitzler and L. Thiele, "Multiobjective evolutionary algorithms: A comparative case study and the strength Pareto approach," *IEEE Trans. Evol. Comput.*, vol. 3, no. 4, pp. 257–271, Nov. 1999.
[63] E. Zitzler, M. Laumanns, and L. Thiele, "SPEA2: Improving the strength Pareto evolutionary algorithm," Swiss Federal Inst. Technol., Rich, Switzerland, Tech. Rep. TIK-Rep. 103, 2001.
[64] K. Deb, A. Pratap, S. Agarwal, and T. Meyarivan, "A fast and elitist multiobjective genetic algorithm: NSGA-II," *IEEE Trans. Evol. Comput.*, vol. 6, no. 2, pp. 182–197, Apr. 2002.
[65] K. Deb and H. Jain, "An evolutionary many-objective optimization algorithm using reference-point-based nondominated sorting approach—Part I: Solving problems with box constraints," *IEEE Trans. Evol. Comput.*, vol. 18, no. 4, pp. 577–601, Aug. 2014.
[66] H. Jain and K. Deb, "An evolutionary many-objective optimization algorithm using reference-point based nondominated sorting approach, part II: Handling constraints and extending to an adaptive approach," *IEEE Trans. Evol. Comput.*, vol. 18, no. 4, pp. 602–622, Aug. 2014.
[67] Q. Zhang and H. Li, "MOEA/D: A multiobjective evolutionary algorithm based on decomposition," *IEEE Trans. Evol. Comput.*, vol. 11, no. 6, pp. 712–731, Dec. 2007.
[68] C.-F. Juang, "A hybrid of genetic algorithm and particle swarm optimization for recurrent network design," *IEEE Trans. Syst. Man, Cybern., B*, vol. 34, no. 2, pp. 997–1006, Apr. 2004.
[69] Y.-T. Kao and E. Zahara, "A hybrid genetic algorithm and particle swarm optimization for multimodal functions," *Appl. Soft Comput.*, vol. 8, no. 2, pp. 849–857, Mar. 2008.
[70] H. Duan, Q. Luo, Y. Shi, and G. Ma, "Hybrid particle swarm optimization and genetic algorithm for multi-UAV formation reconfiguration," *IEEE Comput. Intell. Mag.*, vol. 8, no. 3, pp. 16–27, Aug. 2013.
[71] P. Dziwinski and L. Bartczuk, "A new hybrid particle swarm optimization and genetic algorithm method controlled by fuzzy logic," *IEEE Trans. Fuzzy Syst.*, vol. 28, no. 6, pp. 1140–1154, Jun. 2020.
[72] T. Friedrich, K. Bringmann, T. Voß, and C. Igel, "The logarithmic hypervolume indicator," in *Proc. 11th Workshop Found. genetic algorithms*, New York, NY, USA, Jan. 2011, pp. 81–92.
[73] T. Binh and U. Korn, "MOBES: A multiobjective evolution strategy for constrained optimi-zation problems," in *Proc. 3rd Int. Conf. Genetic Algo-Rithms*, 1997, pp. 176–182.
[74] C. M. Fonseca and P. J. Fleming, "An overview of evolutionary algorithms in multiobjective optimization," *Evol. Comput.*, vol. 3, no. 1, pp. 1–16, Mar. 1995.
[75] F. Kursawe, "A variant of evolution strategies for vector optimization," in *Proc. Int. Conf. Parallel Problem Solving From Nature*, vol. 496. Berlin, Germany: Springer, 1991, pp. 193–197.
[76] C. Poloni, A. Giurgevich, L. Onesti, and V. Pediroda, "Hybridization of a multi-objective genetic algorithm, a neural network and a classical optimizer for a complex design problem in fluid dynamics," *Comput. Methods Appl. Mech. Eng.*, vol. 186, nos. 2–4, pp. 403–420, Jun. 2000.
[77] K. Deb, L. Thiele, M. Laumanns, and E. Zitzler, "Scalable multi-objective optimization test problems," in *Proc. Congr. Evol. Comput. (CEC)*, May 2002, pp. 825–830.
[78] C. A. C. Coello and M. R. Sierra, "A study of the parallelization of a coevolutionary multi-objective evolutionary algorithm," in *Proc. 3rd Mex. Int. Conf. Artif. Intell. (MICAI)*, 2004, pp. 688–697.
[79] A. Mohammadi, M. N. Omidvar, and X. Li, "A new performance metric for user-preference based multi-objective evolutionary algorithms," in *Proc. IEEE Congr. Evol. Comput.*, Jun. 2013, pp. 2825–2832.
[80] J. L. Teugels, "The class of subexponential distributions," *Ann. Probab.*, vol. 3, no. 6, pp. 1000–1011, Dec. 1975.

ANDRANIK S. AKOPOV (Member, IEEE) was born in Russia, in 1974. He received the degree from the Moscow Aviation Institute, in 1997, and the Dr.Sc. degree in engineering from the Russian Academy of Sciences, in 2009. He is currently a Chief Researcher with the Central Economics and Mathematics Institute, Russian Academy of Sciences (RAS), and a Full Professor with the Moscow Institute of Physics and Technology (MIPT) and the MIREA—Russian Technological University. He was awarded by an honorary degree of Professor with the Russian Academy of Sciences in the result of elections to the RAS, in April 2022. His main research interests include agent-based modeling, fuzzy systems, and evolutionary computations.

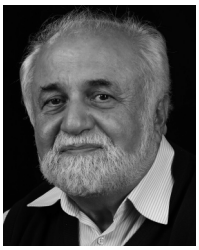

LEVON A. BEKLARYAN was born in Russia, in 1951. He received the degree (Hons.) from Lomonosov Moscow State University (MSU), in 1974, and the Dr.Sc. degree in mathematics from the Russian Academy of Sciences, in 1991. He is currently a Chief Researcher with the Central Economics and Mathematics Institute, Russian Academy of Sciences, and a Full Professor with the Moscow Institute of Physics and Technology (MIPT). His main research interests include dynamic systems, operations research, and optimal control.